© 2019. Published by The Company of Biologists Ltd | Development (2019) 146, dev174938. doi:10.1242/dev.174938

TECHNIQUES AND RESOURCES

RESEARCH ARTICLE

Developmental analyses of mouse embryos and adults using a non-overlapping tracing system for all three germ layers

Takashi Serizawa[1,*], Ayako Isotani[2,3], Takafumi Matsumura[2], Katsuyuki Nakanishi[1], Shigenori Nonaka[4,5], Shinsuke Shibata[1], Masahito Ikawa[2] and Hideyuki Okano[1,*]

ABSTRACT

Genetic lineage-tracing techniques are powerful tools for studying specific cell populations in development and pathogenesis. Previous techniques have mainly involved systems for tracing a single gene, which are limited in their ability to facilitate direct comparisons of the contributions of different cell lineages. We have developed a new combinatorial system for tracing all three germ layers using self-cleaving 2A peptides and multiple site-specific recombinases (SSRs). In the resulting TRiCK (TRiple Coloured germ layer Knock-in) mice, the three germ layers are conditionally and simultaneously labelled with distinct fluorescent proteins via embryogenesis. We show that previously reported ectopic expressions of lineage markers are the outcome of secondary gene expression. The results presented here also indicate that the commitment of caudal axial stem cells to neural or mesodermal fate proceeds without lineage fluctuations, contrary to the notion of their bi-potency. Moreover, we developed IMES, an optimized tissue clearing method that is highly compatible with a variety of fluorescent proteins and immunostaining, and the combined use of TRiCK mice and IMES can facilitate comprehensive analyses of dynamic contributions of all three germ layers.

KEY WORDS: Lineage-tracing system, Fate map, Germ layer, 2A peptide, Site-specific recombinase, Tissue clearing

INTRODUCTION

Specification of the cellular populations responsible for development or pathogenesis has attracted attention in recent decades. Various genetic techniques have been developed for analyses of gene functions and lineage fates. Among them, site-specific recombinases (SSRs), such as Cre, are powerful genetic tools for tracing the specific progeny of cells that once expressed a gene of interest *in vitro* and *in vivo* (Sternberg and Hamilton, 1981; Sternberg et al., 1981; Sauer and Henderson, 1988; Orban et al., 1992).

Recently, several additional SSR systems, such as Flp/*FRT*, Dre/*rox*, VCre/*VloxP*, phiC31/*att*, Vika/*vox*, and Nigri/*nox*, have come into use for the manipulation of two or more distinct genes in eukaryotes (McLeod et al., 1986; Dymecki, 1996; Raymond and Soriano, 2007; Anastassiadis et al., 2009; Suzuki and Nakayama, 2011; Groth et al., 2000; Belteki et al., 2003; Karimova et al., 2013, 2016; Liu et al., 2018). The context for induction of SSRs needs to be considered carefully to enable precise tracing. For example, *Sox17-iCre*;*R26R* mice, in which a codon-improved Cre (iCre) is inserted at the transcriptional start region (TSR) of the first exon in the *Sox17* locus, show endothelial-specific expression of *LacZ* in arteries (Liao et al., 2009), whereas *Sox17-2A-iCre*;*R26R* mice, in which iCre is conjugated to the *Sox17* gene with self-cleaving 2A peptide and the transcript preserves the intact *Sox17* intragenic regions and 3′ untranslated region (UTR) sequence, show more precise and comprehensive expression of *LacZ* in endoderm-derived tissues (Engert et al., 2009). These results indicate that lineage-specific promoters should be introduced with their full context, including their intragenic regions, for precise lineage tracing. It is difficult to directly compare the dynamic contributions of distinct cell lineages using conventional single-gene tracing systems, which occasionally produce ectopic gene expression. Ectopic expression in single-gene tracing systems has been reported in *T-Cre*;*R26R* mice, which show an ectopic β-gal^{+} phenotype in ectodermal tissues, such as lens, caudal neural tube and posterior surface ectoderm (Perantoni et al., 2005), although brachyury (*T*) is well known as a pan-mesodermal marker.

Here, we sought to focus on the development of all three germ layers (ectoderm, mesoderm and endoderm); however, examining the contributions, interactions, trans-differentiation and gene expression orders among these during embryogenesis or in adults can be challenging without the use of invasive manipulations. For this purpose, we developed a new combinatorial lineage-tracing system for visualization of progenies derived from the three germ layers using self-cleaving 2A peptide and multiple SSRs to resolve the issues in the conventional systems outlined above. All three germ layers in the resultant quadruple gene-targeted mice were conditionally and simultaneously labelled with distinct fluorescent proteins. In addition to these technical advances, we provide significant new insights into lineage fate commitments in the current study.

RESULTS

Construct design and generation of TRiCK mice

To specify the three germ layers, we selected *Sox1*, brachyury and *Sox17* as lineage markers for the neuroectoderm, mesoderm and endoderm, respectively (Takashima et al., 2007; Ying et al., 2003; Perantoni et al., 2005; Kumar et al., 2008; Liao et al., 2009; Engert et al., 2009, 2013; Choi et al., 2012; Burtscher et al., 2012). We designed the targeting constructs with a combinatorial system containing self-cleaving 2A peptides and multiple SSRs for labelling the three germ layer markers in an intact gene expression

[1]Department of Physiology, Keio University School of Medicine, Shinjuku, Tokyo 160-8582, Japan. [2]Research Institute for Microbial Diseases, Osaka University, Suita, Osaka 565-0871, Japan. [3]Organ developmental engineering, Division of Biomedical Science, Graduate School of Biological Sciences, Nara Institute of Science and Technology, Ikoma, Nara 630-0192, Japan. [4]Spatiotemporal Regulations Group, Exploratory Research Center on Life and Living Systems (ExCELLS), Okazaki, Aichi 444-8585, Japan. [5]Laboratory for Spatiotemporal Regulations, National Institute for Basic Biology, Okazaki, Aichi 444-8585, Japan.

*Authors for correspondence (serizawa@z7.keio.jp; hidokano@a2.keio.jp)

T.S., 0000-0002-0102-4755; H.O., 0000-0001-7482-5935

Received 15 December 2018; Accepted 30 September 2019

Development (2019) 146, dev174938. doi:10.1242/dev.174938

manner (Fig. 1, Fig. S1). Multiple genes fused with the 2A peptide sequence successfully result in bi-cistronic expression of proteins, as ribosomal skipping caused by the 2A peptide occurs at the conserved core sequence (GDVExNPGP) during translation (Luke et al., 2008). The 2A peptide-mediated expression of multiple proteins has a notable benefit in enabling higher expression levels of proteins compared with IRES (internal ribosome entry site)-mediated expression. Among the common 2A peptides, porcine teschovirus 1 2A (P2A) is reported to have a high cleavage efficiency (Kim et al., 2011; Liu et al., 2017); therefore, we exploited P2A for bi-cistronic expression of SSRs in equimolar amounts to lineage marker genes, and for retaining of their intragenic enhancers, 3′ UTR sequence and poly(A) tail. Next, we used Cre, Dre and a codon-optimized phiC31 (phiC31o; Raymond and Soriano, 2007) as lineage-labelling SSRs, given that all have high recombination efficiencies and do not show cross-reactivity (Fig. S2). As FLP or a codon-optimized FLP (FLPo) has been reported to produce efficient and independent recombination in wild *FRT* or mutant (F3 and F5) sets (Schlake and Bode, 1994), it was also used for simultaneous removal of puromycin-resistance cassettes in different lineage marker alleles *in vivo*. In the reporter construct, multiple fluorescent proteins are flanked by the corresponding recombination target sequences at the *Gt(ROSA)26* locus, under the control of the CAGGS promoter, which enhances ubiquitous expression (Zong et al., 2005). However, their transcription is abrogated by a puromycin-resistance gene, 3-frame stop codons and poly(A) signal for complete prevention of ribosomal read-through before any recombinations (Fig. 1, Fig. S1). Thus, the reporter construct conditionally induces the distinct expression of fluorescent proteins in a lineage marker-dependent manner; i.e. *Sox1* labels neuroectoderm as Venus^{+}, brachyury labels mesoderm as mCherry^{+} and *Sox17* labels endoderm as mCerulean^{+}. Furthermore, this system can change colours from mCherry (brachyury^{+} mesendoderm) to mCerulean (*Sox17*$^{+}$ endoderm) in response to further lineage specification.

Homologous recombination of the ROSA reporter allele (designated as *ROSA26*^{MultiFPs}) and three lineage-labelling alleles (designated as *Sox1*$^{2A\text{-}Cre}$, brachyury$^{2A\text{-}Dre}$ and *Sox17*$^{2A\text{-}phiC31o}$) in the puromycin-resistant mES clones was confirmed by Southern blotting analysis or PCR-based genotyping methods (Fig. S1E,F). For chimeric mice production, we selected clones 1, 25 and 26 (all homozygous) as the ROSA reporter mES clones, and clones 49 (homozygous for brachyury and *Sox17*, and heterozygous for *Sox1*) and 2–3 (homozygous for *Sox1* and *Sox17*, and heterozygous for brachyury) as the triple lineage-labelling mES clones. Chimera mice were generated by injection to eight-cell stage ICR embryos, and the chimeric contributions of the injected mES clones were estimated using the coat colours of chimeras. For both lines, high chimeric F0 males were crossed with CAG-FLPo (Yamazaki et al., 2016) females to remove puromycin-resistance cassettes in the targeted genes for restoration of their intact 3′ UTR sequences and poly(A) tails. Following the initial crossing, we genotyped the F1 mice to confirm germline transmissions. Among them, we chose clone 26 and 2-3 derivatives (designated as *ROSA26*^{MultiFPsΔPuro} and the triple lineage-labelling mice, respectively) owing to the stable production of the offspring. For *ROSA26*^{MultiFPsΔPuro}, the heterozygous mice were inbred, and a homozygous line was established. For the triple lineage-labelling mice, males heterozygous for all lineage markers were selected. Finally, we crossed the triple lineage-labelling males (*Sox1*$^{2A\text{-}CreΔPuro/+}$, brachyury$^{2A\text{-}DreΔPuro/+}$ and *Sox17*$^{2A\text{-}phiC31oΔPuro/+}$) to *ROSA26*$^{MultiFPsΔPuro/MultiFPsΔPuro}$ females to obtain the objective mice. We designated such quadruple gene-targeted mice as TRiCK (TRiple Coloured germ layer, Knock-in) mice.

Analyses of the developing embryos

We first validated the lineage-tracing phenotype of the TRiCK mice in developing embryos. To this end, we mated the two mouse lines as described above, expecting that TRiCK mice would be produced with a probability of one-eighth. As a preliminary experiment, we dissected a pregnant mouse and obtained ten E14.5 embryos; these displayed the different combinations of fluorescent protein expressions (Fig. 2A). Among them, one TRiCK mouse simultaneously showed non-overlapping and conditional labelling in all three germ layers (Fig. 2B), in which the brain, spinal cord and eyes were Venus^{+}, the trunk was mCherry^{+}, and mCerulean^{+} cells were scattered across the surface of the whole body. We next sought to examine the temporal patterning in the early development of TRiCK mouse embryos. The E8.5 embryo showed Venus^{+} neural plate surrounded with mCherry^{+} mesodermal cells (Fig. 2C). mCerulean^{+} endodermal cells were detected in the caudal part of the embryo. The TRiCK mouse embryos displayed the dynamic lineage specifications at E9.5 and E10.5, with the formation of Venus^{+} neural tube and optic vesicles, mCherry^{+} somites and organ buds, and definite commitment to mCerulean^{+} endoderm in the branchial arches (Fig. 2D,E). We also confirmed the specificity of the TRiCK system using a littermate embryo that did not show any fluorescent

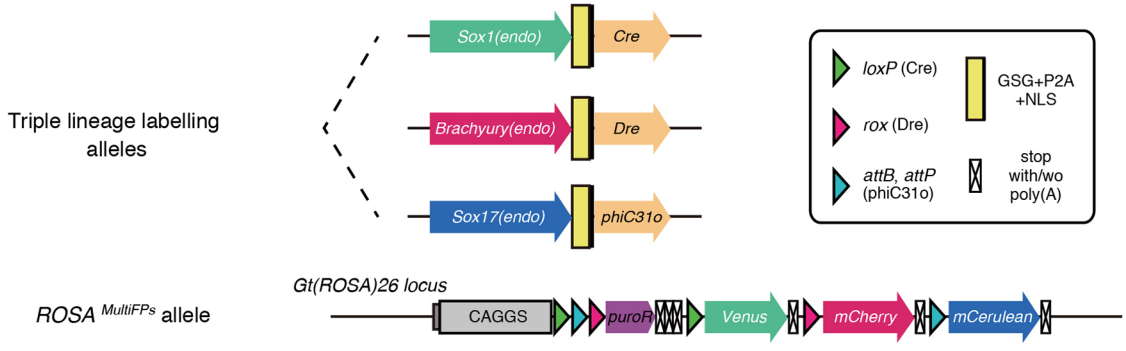

Fig. 1. Schematic view of the TRiCK system. Each germ layer marker gene (*Sox1*, brachyury and *Sox17*) induces the distinct site-specific recombinase (SSR) in the manner of self-cleaving 2A peptide-mediated bi-cistronic expression. Multiple fluorescent proteins are inserted into the constitutively active genomic locus at *Gt(ROSA)26* under the control of ubiquitous CAGGS promoter. Before any SSR-mediated recombination, the transcription is terminated by a puromycin-resistance gene (*puroR*), 3-frame stop codons and poly(A) signal. During embryogenesis, the distinct fluorescent protein is activated by each SSR responding to the germ layer marker gene expression.

Development (2019) 146, dev174938. doi:10.1242/dev.174938

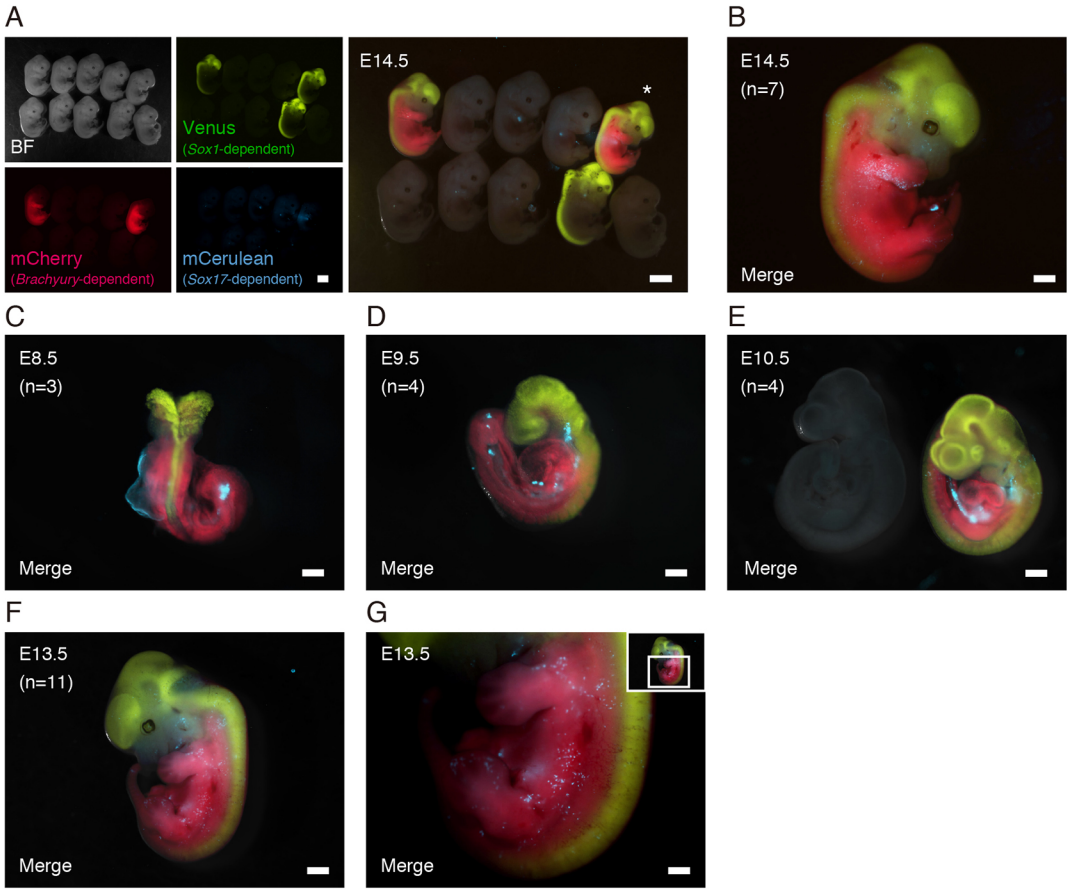

Fig. 2. TRiCK mice simultaneously show distinct lineage labelling in developing embryos. The *ROSA*$^{MultiFPs\Delta Puro/MultiFPs\Delta Puro}$ pregnant females crossed to the triple lineage-labelling males (*Sox1*$^{2A\text{-}Cre\Delta Puro/+}$, *Brachyury*$^{2A\text{-}Dre\Delta Puro/+}$ and *Sox17*$^{2A\text{-}phiC31o\Delta Puro/+}$) were dissected at each day post-coitum. *Sox1*$^{2A\text{-}Cre\Delta Puro}$ drove Venus (green); *Brachyury*$^{2A\text{-}Dre\Delta Puro}$ drove mCherry (red); and *Sox17*$^{2A\text{-}phiC31o\Delta Puro}$ drove mCerulean (cyan). (A) The resulting E14.5 embryos displayed the distinct combinations of the fluorescent proteins. Asterisk indicates a TRiCK embryo that was simultaneously labelled in all three germ layers. (B) The magnified image of the E14.5 TRiCK embryo as shown in A (asterisk). (C-G) Temporal lineage specifications were analysed at each developmental stage: E8.5 (C), E9.5 (D), E10.5 (E, right) and E13.5 (F,G). A littermate E10.5 embryo (left, negative control) did not show any fluorescent signals at all wavelengths (E). The TRiCK embryos maintained the definite labelled boundaries between three germ layers until late stage development (G; a magnified image of F). BF, bright field. Scale bars: 2 mm in A; 1 mm in B,F; 500 µm in E,G; 200 µm in C,D. Representative images of biological specimens are presented; *n* is the total number of embryos we examined.

signals as a negative control (Fig. 2E). The TRiCK mouse embryos precisely maintained the fluorescent boundaries of the three germ layers until late development (Fig. 2B,F,G).

Development of the IMES tissue clearing solution for 3D imaging of embryos

We next sought to analyse TRiCK embryos using recently developed 3D imaging techniques for detailed analyses of dynamic lineage specifications during embryogenesis. Many techniques for tissue clearing, such as CLARITY, PACT, 3DISCO, Sca*l*e, Sca*l*eS, CUBIC, SeeDB and SeeDB2 (Chung et al., 2013; Treweek et al., 2015; Becker et al., 2012; Hama et al., 2011, 2015; Susaki et al., 2014; Ke et al., 2013, 2016), have been reported. These techniques are beneficial for spatial mapping of diverse cell populations and understanding their biological relationships. However, these techniques often induce a decline in fluorescent protein (XFP) signals during the clearing performance. One of the solutions to this issue is signal enhancement by XFP-specific antibodies; however, it is difficult to independently detect all XFPs used in the TRiCK system with antibodies, as Venus and mCerulean have highly preserved their protein sequences (230 of 239 amino acids are identical). Furthermore, the commercially available anti-GFP antibodies crossreact with both GFP/YFP (Venus) and CFP (mCerulean). Therefore, it is important to retain the intact XFP signals during the tissue clearing process.

As the first step for improving tissue clearing, we investigated the optimal fixation protocol, as the common fixation condition, 4% paraformaldehyde (PFA) in PBS, resulted in decreased XFP intensities and significantly increased background, especially at short wavelengths. We compared several concentrations of PFA, diluent buffers and additive combinations. Then, we observed the highest performance in preservation of XFP signals when we used 0.5-2% PFA diluted with PHEM buffer (pH adjusted to 8.0) instead of PBS. Furthermore, the addition of 5% D-sorbitol effectively suppressed the increase of auto-fluorescence during fixation (data not shown).

Next, we optimized the tissue clearing method. We started by evaluating the performance of Sca*l*e U2 and S4 solutions as promising previous techniques, because their aqueous-based methods are expected to be mild for XFPs (Hama et al., 2011, 2015). However, when we immersed the fixed E13.5 TRiCK embryo in Sca*l*e U2 or S4 solution, we observed a decrease in XFP

Development (2019) 146, dev174938. doi:10.1242/dev.174938

signals and the accumulation of auto-fluorescence at short wavelengths that overlap with mCerulean detection (data not shown). To handle this issue, we focused on the SeeDB2 method (Ke et al., 2016), which is designed to preserve most of the XFP signals, and is based on the high refractive index (RI) of iohexol, usually used as a clinical contrast medium (e.g. Omunipaque350). The samples immersed in SeeDB2 medium showed partial transparency, which was insufficient for whole-embryo imaging (Fig. 3A). However, SeeDB2 controlled auto-fluorescence at low levels during the clearing process (data not shown). We also evaluated the Ce3D method (Li et al., 2017), which uses Histodenz, a brand of iohexol, as an alternative, but, unexpectedly, it caused extreme sample shrinkage in our hands (Fig. 3A). Therefore, we proceeded to screen the original additives in combination with iohexol for enhancement of tissue transparency with preservation of soft tissue structures. We compared several chemicals in general laboratory use, and found that the addition of monoethanolamine (MEA) delivered superior tissue transparency without obvious tissue deformation or decrease in XFP signals. Notably, triethanolamine did not show any transparency enhancement in combination to iohexol, although it was reported to be effective for tissue clearing in Sca*l*eCUBIC-2 medium (Susaki et al., 2014). Further experiments indicated that D-sorbitol and EDTA can also contribute to the retention of XFP signals. We named the final formulation of tissue clearing solution IMES (iohexol, monoethanolamine, EDTA, sorbitol-based clearing) solution. The IMES method achieved high performance in tissue transparency with preservation of intact structures (Fig. 3A).

We immersed the fixed E13.5-14.5 TRiCK embryos in IMES solution and processed clearing, confirming that it is compatible with all XFPs in the system. The cleared TRiCK embryo showed almost completely complementary expression of XFPs throughout the entire body (Fig. 3B, Movie 1), but some cell populations were positive for both mCherry and mCerulean (Fig. 3C arrowheads). In the tongue, mCherry^{+} muscle cells were arranged in a line and lay beside the Venus^{+} cells, including gustatory nerves (Fig. 3D, Movie 2). We also confirmed that numerous Venus^{+} cells dispersed throughout the connective tissues of the head. Moreover, we could clearly distinguish the cell populations of different cell origins in the eye (Fig. 3E). Thus, we validated that TRiCK mice can potentially become a powerful tool in analyses of dynamic developmental relationships between the three germ layers when combined with tissue clearing methods, especially the IMES technique.

Analyses of the adult organs

The TRiCK mice showed no abnormalities at birth, and grew to adults. We next examined contributions of three germ layers in different organs of over 8-week-old adults. The brain and spinal

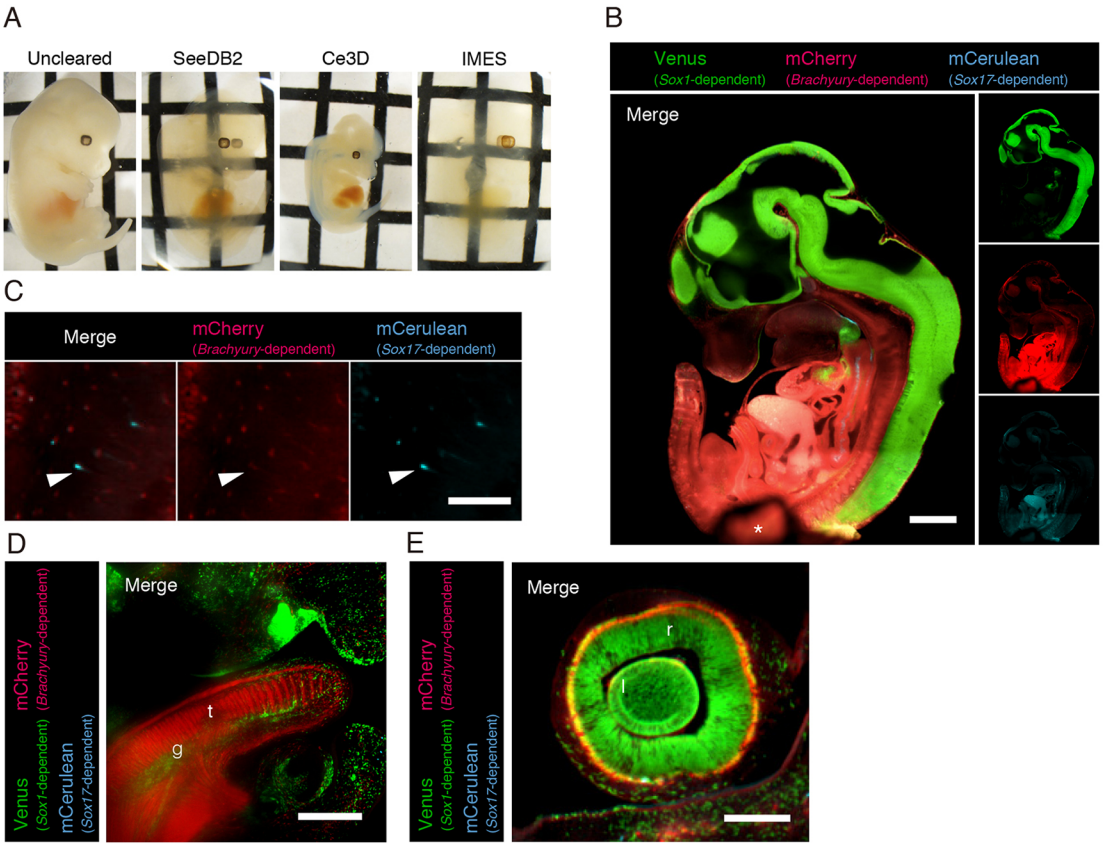

Fig. 3. An optimized clearing method, IMES, demonstrates the simultaneous observation of all three lineage labels in TRiCK embryos. We optimized the tissue clearing method, IMES (iohexol, monoethanolamine, EDTA, sorbitol-based clearing), and E13.5-14.5 TRiCK embryos were cleared using this method. (A) A comparison of the previously reported methods, SeeDB2 and Ce3D, which use iohexol as their high RI reagent, with IMES. IMES outperformed in tissue transparency without tissue deformation. Grid size: 3.3 mm. (B) A virtual sagittal section image of a cleared E13.5 TRiCK embryo under lightsheet microscopy. Asterisk indicates the position used to hold the specimen. (C) Magnified image in the spinal cord of an E13.5 TRiCK embryo. Arrowhead indicates a cell that is double positive for mCherry and mCerulean. (D,E) Detailed observation in the tongue at E14.5 (D) and in the eye at E13.5 (E) of a TRiCK embryo. *Sox1*$^{2A\text{-}Cre\Delta Puro}$ drove Venus (green); *Brachyury*$^{2A\text{-}Dre\Delta Puro}$ drove mCherry (red); and *Sox17*$^{2A\text{-}phiC31o\Delta Puro}$ drove mCerulean (cyan). t, tongue; g, gustatory nerve; l, lens; r, retina. Scale bars: 1 mm in B; 200 µm in C,E; 500 µm in D. Representative images of three individual biological specimens are presented.

Development (2019) 146, dev174938. doi:10.1242/dev.174938

cord entirely expressed Venus; however, it was remarkable that mCherry^{+} cells and mCerulean^{+} cells were also conspicuously present throughout the brain (Fig. 4). As microglia originates from yolk-sac mesoderm (Kierdorf et al., 2013; Hoeffel et al., 2015) and brachyury is co-expressed with the classical microglial marker IBA-1 during *in vitro* differentiation to microglia (Ormel et al., 2018), we performed immunostaining for IBA-1 on floating brain slices and subsequently cleared using the IMES method. Nearly all IBA-1-positive cells were also labelled with mCherry (Fig. S3A,B), suggesting that microglia emerge from the brachyury-positive mesodermal cell population. Interestingly, mCherry^{+} microglia strongly accumulated at cerebellar sulci and resided along veins (Figs 4 and 5A,B). Although veins showed no detectable fluorescence (Fig. 5B), capillary arteries could be visualized with

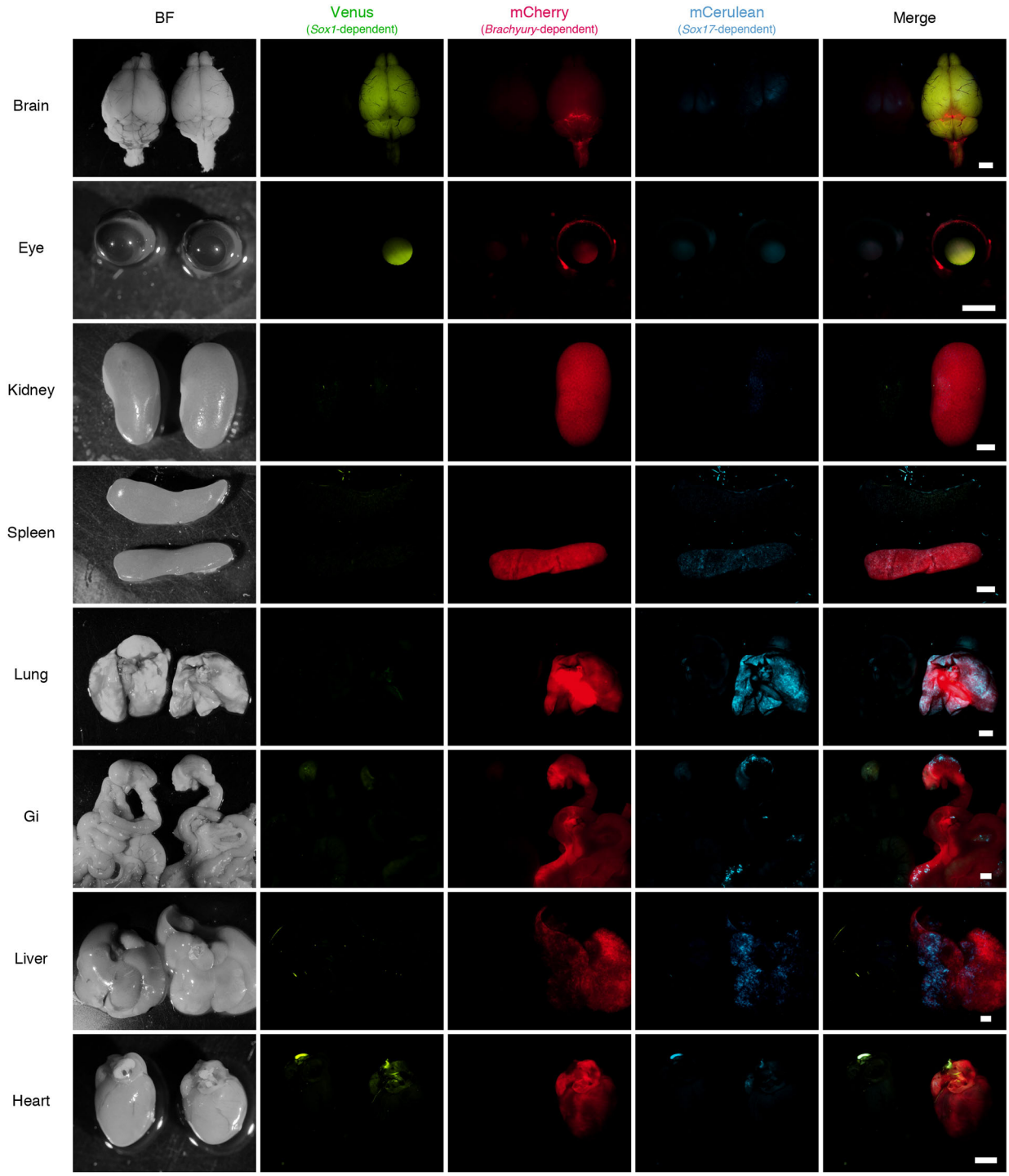

Fig. 4. Comparison of fluorescent protein expression in different organs in adult TRiCK mice. The male TRiCK mice were dissected at 8 weeks. We could readily distinguish the different lineage progenies in each organ by detecting their fluorescent signals (right). *Sox1*$^{2A\text{-}Cre\Delta Puro}$ drove Venus (green); *Brachyury*$^{2A\text{-}Dre\Delta Puro}$ drove mCherry (red) and *Sox17*$^{2A\text{-}phiC31o\Delta Puro}$ drove mCerulean (cyan). The littermate mouse did not show any specific signals in any organ (left, negative control). Gi, gastrointestinal tract; BF, bright field. Scale bars: 2 mm. Representative images of five individual biological specimens are presented.

Development (2019) 146, dev174938. doi:10.1242/dev.174938

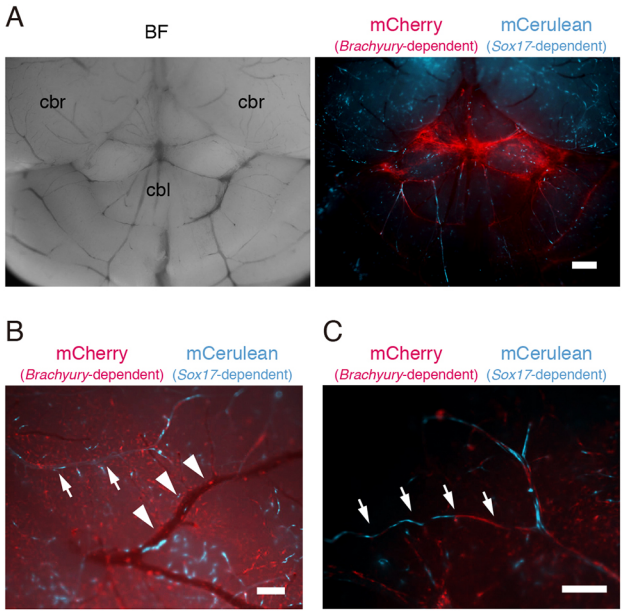

Fig. 5. Mesodermal mCherry$^+$ cells and endodermal mCerulean$^+$ cells are detected throughout the entire brain in adult TRiCK mice. In addition to the uniform Venus expression driven by the neuroectodermal marker *Sox1* in the brain of the TRiCK mouse, we also detected conspicuous populations of mCherry$^+$ or mCerulean$^+$ cells throughout the entire brain, indicating that they were mesodermal or endodermal origin, respectively. *Brachyury*$^{2A\text{-}Dre\Delta Puro}$ drove mCherry (red) and *Sox17*$^{2A\text{-}phiC31o\Delta Puro}$ drove mCerulean (cyan). (A) mCherry$^+$ mesodermal cells were strongly accumulated in cerebellar sulci, in addition to their sparse distribution throughout the brain. cbr, cerebrum; cbl, cerebellum. (B) Capillary endothelial cells of the arteries in the brain surface were labelled with mCerulean (arrows) and mCherry$^+$ cells surrounded the veins (arrowheads), although the veins were not labelled. (C) Incomplete recombination resulting in the mosaic expression pattern of mCherry and mCerulean was observed in the capillary artery (arrows). BF, bright field. Scale bars: 500 µm in A; 200 µm in B,C. Representative images of five individual biological specimens are presented.

both mCerulean$^+$ and mCherry$^+$ endothelial cells, which might be the result of incomplete recombination by *Sox17*-driven phiC31o (Fig. 5B,C). Therefore, we further evaluated the recombination efficiency of phiC31o in brain capillaries that could be stained with the endothelial cell marker PECAM-1. By calculating the ratio of mCerulean$^+$/PECAM-1$^+$ cells to mCherry$^+$/PECAM-1$^+$ cells (Fig. S3C), we estimated phiC31o-mediated recombination in brain endothelial cells occurred at an average efficiency of 76% (Table 1).

Table 1. Calculation for recombination efficiency mediated by phiC31o in brain capillaries

		Animal 1	Animal 2	Animal 3	Average
phiC31o recombination efficiency (%)	Counted by object volume	62.7	85.6	81.0	76.4
	Counted by object number	60.3	86.0	83.2	76.5

TRiCK mouse brain slices (over 200 µm) were immunostained using anti-PECAM1 antibody. Double-positive mCherry$^+$/PECAM-1$^+$ or mCerulean$^+$/PECAM-1$^+$ cells in the cortex were detected using confocal microscopy, and the ratio of mCerulean$^+$ endothelial cells to mCherry$^+$ cells was calculated by object volume and numbers, as an index for the efficiency of phiC31o-mediated recombination in the brain. Each value is for an individual specimen and is the mean of three areas of the cortex.

Since it has been previously reported that the lenses and retina are *Sox1* positive during embryogenesis (Kamachi et al., 1998; Nishiguchi et al., 1998), these were labelled with *Sox1*-dependent Venus (Fig. 4). Furthermore, connective tissues at eye rims, extraocular muscles and some corneal stromal cells were mCherry$^+$ (Fig. 4, Fig. S4A). Consistent with their mesodermal origins, kidney and spleen uniformly displayed mCherry expression (Fig. 4). We observed a mosaic pattern of both mCherry$^+$ and mCerulean$^+$ cells in the lung (Fig. 4). Moreover, mCherry was intensely expressed in the trachea, and Venus$^+$ peripheral nerves extended on its surface (Fig. 4, Fig. S4B). The peripheral nerves were also clearly visualized with Venus in the thoracic domain (Fig. S4C). In the gastrointestinal tract, nearly all cells were mCherry$^+$, and the spotted clonal signals of mCerulean$^+$ cells were also present at the greater curvature of the stomach and small parts of the intestine (Fig. 4). Notably, we also confirmed Venus$^+$ labelling in the enteric nervous system (Fig. S4D).

The liver expressed both mCherry and mCerulean in a mosaic pattern with the different proportions in lobes, and we confirmed both mCherry$^+$ and mCerulean$^+$ cells mostly co-expressed a hepatocyte marker HNF4α (Figs 4 and 6A, Fig. S5, upper).

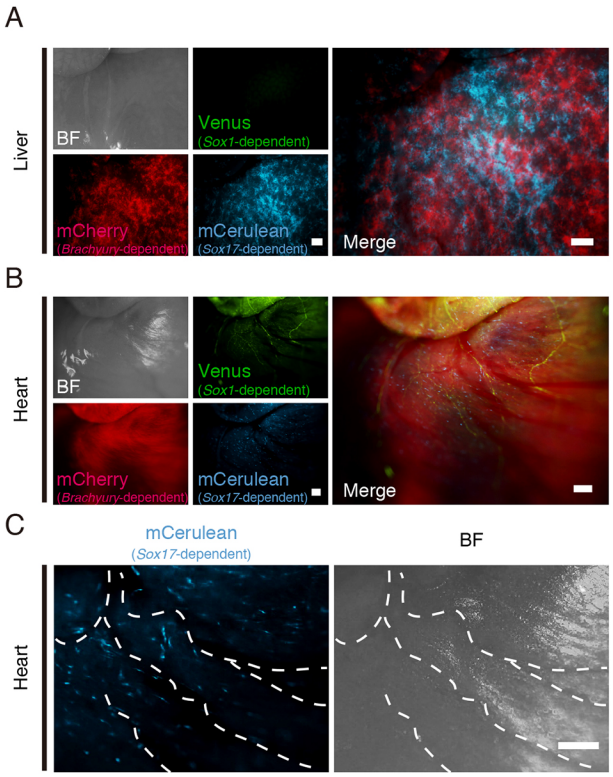

Fig. 6. TRiCK mice show incomplete lineage labels in liver and heart. The livers and hearts of TRiCK mice had a mosaic or marbled expression pattern of fluorescent proteins. *Sox1*$^{2A\text{-}Cre\Delta Puro}$ drove Venus (green); *Brachyury*$^{2A\text{-}Dre\Delta Puro}$ drove mCherry (red); and *Sox17*$^{2A\text{-}phiC31o\Delta Puro}$ drove mCerulean (cyan). (A) The liver showed both mCherry$^+$ and mCerulean$^+$ cellular populations, as shown in Fig. 4. Notably, we observed a considerable cell population that was negative for all lineage labels in the liver. (B) The heart showed a marbled pattern of mCherry$^+$ cells, in addition to Venus$^+$ cardiac nerves and sparse mCerulean$^+$ cells. We also found a cell population that was negative for all lineage labels in the heart, similar to those in the liver. (C) We detected numerous mCerulean$^+$ cells in the surface of the whole heart. mCerulean$^+$ cells resided in an independent pattern to coronary artery routes (white dotted lines). BF, bright field. Scale bars: 500 µm in A; 200 µm in B,C. Representative images of five individual biological specimens are presented.

Development (2019) 146, dev174938. doi:10.1242/dev.174938

To our surprise, the mCherry^{-}/mCerulean^{-} double-negative hepatocytes were present in a considerable cell population of TRiCK mouse liver. To investigate this phenotype, we considered the possibility of XFP degradation using XFP-specific antibodies. While anti-RFP antibody staining showed complete colocalization with mCherry signals (Fig. S5, middle), anti-GFP antibody (it recognizes Venus and mCerulean in this system, but Venus expression was not detectable in the liver) staining resulted in some different profiles. Strong anti-GFP signals coincided with mCerulean expression (Fig. S5, bottom, arrows). In contrast, the cells with weak anti-GFP signals did not express definite mCerulean signals, or only expressed the minimum for detection (Fig. S5, bottom, arrowheads). These results indicate the hepatocytes, which were apparently negative for all lineage labels, partly resulted from the protein degradation of mCerulean.

We observed a more complex phenotype in the heart, in which mCherry was expressed in a marbled pattern throughout the entire organ, Venus labelled the cardiac nerves and numerous mCerulean^{+} cells were dispersed on the surface of the heart in an independent pattern to coronary artery routes (Figs 4 and 6B,C). We identified mCherry^{+} cell population as TNNI3^{+} cardiomyocytes (Fig. S6A). As for mCerulean^{+} cells, *Sox17* is activated in the haematopoietic stem cells (HSCs) giving rise to foetal macrophages (Engert et al., 2009); HSC-derived cardiac macrophages reside in the adult heart (Epelman et al., 2014; Frantz and Nahrendorf, 2014). Therefore, we immunostained heart tissues with macrophage markers, such as CD11b and F4/80; however, none of these markers was co-expressed with mCerulean signals (data not shown). For further exploration, we tested colocalization of mCerulean and PECAM-1 with signal enhancement by anti-GFP antibody; mCerulean (anti-GFP signal)-positive cells mostly coincided with PECAM-1-positive capillaries in the heart (Fig. S6B). Consequently, we identified these cells as turned out endothelial cells. Moreover, we discovered there was an exceptional cell population, similar to that in the liver, that was negative for all lineage labels (Fig. 6B). However, these non-labelled cells were negative for anti-RFP antibody (Fig. S6C), which suggests that the protein degradation of mCherry was not involved in its marbled expression pattern.

We also examined the fluorescent phenotype in gonads. The testis expressed only mCherry, however, the ovary and uterus expressed punctate mCerulean signals, in addition to mCherry signal in the entire organs (Fig. 7). TRiCK mice were fertile and their offspring showed whole-body mCherry^{+} phenotype (data not shown), consistent with the initial involvement of brachyury to germ cell lineage commitment in mice, as previously described (Aramaki et al., 2013).

DISCUSSION

Here, we report a new combinatorial system using self-cleaving 2A peptides and multiple SSRs for triple lineage fate tracing, as well as a new tissue clearing method that preserves XFP intensities, with a particular focus on the development of the three germ layers. As conventional single-gene tracing systems have difficulties in comparing the contributions of different lineage populations, and in determining the sequential gene expression orders of different lineage markers, we designed a quadruple knock-in system to resolve these issues. In this system, three germ layers (neuroectoderm, mesoderm and endoderm) can be labelled conditionally and simultaneously by using distinct fluorescent proteins that label *Sox1*, brachyury and *Sox17* gene expressions. To validate the system, we analysed the phenotype of the resultant quadruple gene-targeted (TRiCK) mice, as developing embryos and adults.

We confirmed that, in most instances, TRiCK mice precisely maintain the boundaries of multiple lineage progenies labelled with distinct fluorescent proteins in bona fide patterns that are consistent with the results from conventional single-gene tracing systems. As an exception, TRiCK embryos partly possessed a cell population double-positive for mCherry^{+} and mCerulean^{+} (Fig. 3C). However, because adult TRiCK mice over 8 weeks old did not show any overlap of XFP expression in any organ (Figs 4–7, Figs S3–S6), we concluded this phenotype in the developing embryo was due to the retention of mCherry protein, although its translation had been terminated by phiC31o-mediated recombination. Therefore, we considered that these cells were in transition from mCherry^{+} to mCerulean^{+} phenotype. In addition, there were some particular characteristics of the TRiCK mice that differed from the previous single-gene-tracing models. For example, the lenses and caudal neural tube were completely visualized with *Sox1*-driven Venus (Fig. 2B-G), although these tissues were reported to be labelled in *T* (brachyury)-*Cre*;*R26R* mice (Perantoni et al., 2005). These results point to the possibility that the previously reported ectopic expressions of lineage markers are the outcome of secondary gene expression. As the caudal neural tube was solely labelled with *Sox1*-

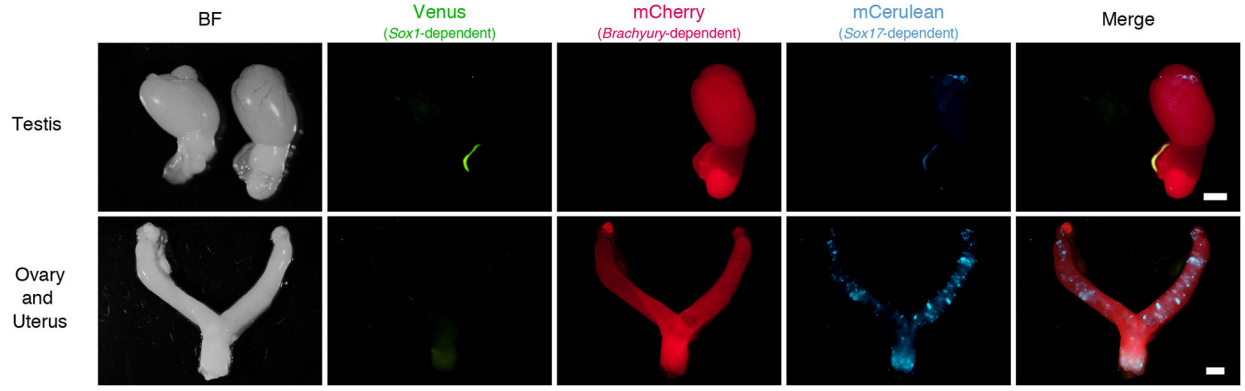

Fig. 7. Gonad labelling in TRiCK mice. Gonads showed dominant mCherry expression both in male and female TRiCK mice. *Sox1*$^{2A\text{-}Cre\Delta Puro}$ drove Venus (green); *Brachyury*$^{2A\text{-}Dre\Delta Puro}$ drove mCherry (red); and *Sox17*$^{2A\text{-}phiC31o\Delta Puro}$ drove mCerulean (cyan). The testis displayed uniform mCherry expression (right). The littermate mouse did not show any specific signals (left, negative control). The ovary and uterus displayed the spotted mCerulean expression, although they both strongly displayed the entire mCherry expression. BF, bright field. Scale bars: 2 mm. Representative images of five individual biological specimens are presented.

Development (2019) 146, dev174938. doi:10.1242/dev.174938

driven Venus at E10.5 and later stages, in which the caudal axial stem cells have already shown their bi-potency to neural or mesodermal fates in *Tbx6*-KO mice (Takemoto et al., 2011), our results indicate that the lineage fate commitment of the caudal axial stem cells proceeds without lineage fluctuations. Thus, it is important to determine the order of gene expression for a better understanding of bona fide cellular origins or organ development.

It was also interesting that considerable cell populations, which were negative for all three lineage markers, could be observed in the liver and heart (Figs 4 and 6, Figs S5 and S6). While we observed that protein degradation of XFPs, especially with mCerulean, was partly related to this phenotype in the liver (Fig. S5), this would not affect mCherry detection in the liver and heart (Figs S5 and S6). These results are consistent with a previous study that referred to the possibility of incomplete recombination in the heart of *T* (brachyury)-*Cre*;*R26R* mice embryo (Perantoni et al., 2005). However, as mCherry^{+} mesendoderm differentiates to mCherry^{+} mesoderm or mCerulean^{+} endoderm in the TRiCK system, mesendoderm-derived tissues should express either mCherry or mCerulean. Thus, these cell populations appear never to have expressed brachyury at sufficient transcriptional levels for recombination throughout their lineage fate commitments from mesendoderm. Moreover, there are additional possible explanations, such as gene silencing of the reporter gene allele or that the cytotoxicity of SSRs or XFPs causes elimination of the recombined cells or the reporter gene allele. Notably, the marbled fluorescent pattern observed in the heart suggests that the non-labelled population was specified early in heart development, and that these cells clonally proliferated and maintained the quiescent mode for brachyury expression. We should further explore whether there are physiological differences between the labelled and non-labelled cell populations.

We detected incomplete recombination of *Sox17*-driven phiC31o in capillary endothelial cells (Fig. 5C, Fig. S3C, Table 1) and other endodermal tissues. As we also observed the relative low recombination efficiency of phiC31o *in vitro* compared with Cre and Dre (Fig. S2), this is a major issue that needs to be improved in the TRiCK system. In such circumstances, other efficient and incompatible SSR systems, e.g. the recently developed Vika/*vox* (Karimova et al., 2013) or Nigri/*nox* (Karimova et al., 2016; Liu et al., 2018), can be used to perform multiple genetic manipulations as replacements for conventional SSRs and/or the combinatorial genetic tool that enables labelling of a fourth target population, such as the neural crest lineage. In addition, *Brachyury*$^{2A\text{-}Dre\Delta Puro}$ homozygous mice exhibit the short tail phenotype and die before adulthood (data not shown), as is typical of brachyury-KO mice (Pennimpede et al., 2012). All lineage marker alleles targeted in the TRiCK system could be maintained as homozygous because 2A peptide-mediated protein cleavages support endogenous gene expression. However, our results suggest that 2A cleavage was not highly effective or that the cleaved fragment of 2A peptide influenced the function of the brachyury protein.

Moreover, the value of TRiCK mice is significantly increased when combined with recently developed tissue clearing methods for comprehensive analyses of diverse cell populations. To this end, we also developed a new aqueous-based clearing method, named IMES, in which MEA is one major component (20 v/v% in IMES) in the clearing step. Although the mechanism needs to be further clarified, MEA enhanced the decolouring process and improved the permeabilization of high RI-matched clearing solution into samples. It is noteworthy that such a high concentration of MEA did not cause tissue shrinkage, unlike *N*-methylacetamide used in the Ce3D method, but over 40 v/v% of MEA resulted in a dramatic loss of XFP signals (data not shown). The optimal formulation of IMES solution generates the high tissue transparency that is sufficient for three-dimensional lightsheet observations within 1 week, with preservation of intact XFP signals, including CFP, and with the lower background levels, which have not been achieved using previous methods.

The TRiCK mice described here can simultaneously visualize and distinguish cells derived from all three germ layers without the use of invasive manipulations. Notably, this system also sheds light on the mechanism for lineage fate commitment of caudal axial stem cells. In addition, we were able to readily distinguish intriguing cell types and tissues, such as microglia, capillary endothelium in the brain and heart, and the peripheral nervous network of each organ in the TRiCK mice. This may also be helpful in analysing temporal and spatial contributions of multiple cell lineages in pathogenesis, e.g. the bilateral characters of microglia and vascular remodelling after cerebral infarction (Mabuchi et al., 2000; Hu et al., 2012; Perego et al., 2011; Kanazawa et al., 2017). Moreover, the combination of TRiCK mice and the IMES clearing method enables the simultaneous multi-colour visualization of three germ layers and immunostained targets, which may facilitate the understanding of diverse cellular relationships. Thus, we expect that TRiCK mice will contribute to progress in the study of development, regeneration and pathogenesis.

MATERIALS AND METHODS

All animal experiments were approved by the Institutional Animal Experiment Committee of Keio University (approval number 09091) and Osaka University (approval number Biken-AP-H25-02).

Cell culture

The C57B6/N and C57B6/J hybrid mouse embryonic stem (mES) cell line B6NJ-22^(UTR) (RIKEN BioResouce Research Center, AES0141; Tanimoto et al., 2008) were cultured at 37°C in 5% CO_2 under feeder-free conditions in N2B27 medium consisting of DMEM/F12 (Fujifilm Wako) and Neurobasal medium mixed at a 1:1 ratio supplemented with 1% N2 supplement, 2% B27 supplement, 2 mM L-glutamine, 0.1 mM NEAA, 1 mM sodium pyruvate (all from Thermo Fisher Scientific), 0.1 mM 2-ME (Sigma), 1000 U/ml hLIF (Merck Millipore), 1 µM PD0325901 (Cayman), 3 µM CHIR99021 (Cayman), 10 ng/ml hBMP4 (HumanZyme) and 10 mM SB431542 (Sigma) on 0.1% gelatinized dish. HEK293T cells were maintained in DMEM (Sigma) supplemented with 10% FBS (Sigma).

Vector construction

Targeting vectors were designed as shown in the figures (Fig. 1, Fig. S1). Briefly, a ROSA26 reporter plasmid was constructed according to standard cloning methods using the following elements: CAGGS promoter (pCAGGS-Cre; RIKEN BioResouce Research Center, RDB08998; Ogawa et al., 2006), Venus, a variant of yellow fluorescent protein with fast and efficient maturation for cell-biological applications (Nagai et al., 2002) derived from pTP1-Venus (Kohyama et al., 2005), mCherry (pG-PB-Zscan4c-mCherry-polyAfloxPGKneo, a gift from Minoru Ko, Keio University School of Medicine, Japan), mCerulean (Cerulean, a gift from Dave Piston, Washington University School of Medicine, USA; Addgene plasmid #15214; Rizzo et al., 2004), puromycin-resistance gene (*puroR*) and *FRT*-PGK/em7-*puroR*-*FRT* (pCAGGS-dre-ires-puro, a gift from A. Francis Stewart, Technische Universität Dresden, Germany; Anastassiadis et al., 2009) and pBTloxP (a gift from Takeshi Yagi, Osaka University, Japan; Yokota et al., 2011). The 5′ and 3′ homology arms for bacterial artificial chromosome (BAC) recombination, SSR target sequences, Kozak sequence and 3-frame stop codons were synthesized with primer extension techniques and then cloned. ROSA26 reporter plasmid was recombined to C57B6/N mouse BAC clone (RIKEN BioResouce Research Center, B6Ng01-316F09), and retrieved to a minimal vector using the Red/ET system (Gene Bridges). Sox1,

Development (2019) 146, dev174938. doi:10.1242/dev.174938

brachyury and Sox17 lineage-labelling plasmids were constructed according to standard cloning methods using the following elements: Cre (pCAGGS-Cre; RIKEN BioResouce Research Center, RDB08998; Ogawa et al., 2006), Dre (pCAGGS-dre-ires-puro, a gift from A. Francis Stewart; Anastassiadis et al., 2009), phiC31o (pPGKPhiC31obpA, a gift from Philippe Soriano, Icahn School of Medicine at Mount Sinai, USA; Addgene plasmid #13795; Raymond and Soriano, 2007). The 5′ and 3′ homology arms for BAC recombination, in-frame GSG (Gly-Ser-Gly)-linker plus P2A and 2×SV40 nuclear localization signal (NLS) sequence were synthesized with primer extension techniques, and PGK/em7-*puroR* flanked by *FRTs* (*FRT*/*F3*/*F5*) was amplified by polymerase chain reaction (PCR) and then cloned. Sox1, brachyury and Sox17 lineage-labelling plasmids were recombined to B6N mouse BAC clones (RIKEN BioResouce Research Center, B6Ng01-307M06, B6Ng01-307A03, and B6Ng01-211A18, respectively), and retrieved to minimal vectors with Red/ET system. For constructing expression vectors of streptococcus pyogenes Cas9 D10A mutant (Cas9 nickase) and guide RNA (gRNA), a synthesized gRNA sequence designed to each target site was cloned to pSpCas9n(BB)-2A-Puro (a gift from Feng Zhang, Broad Institute of Massachusetts Institute of Technology and Harvard, USA; Addgene plasmid #62987; Ran et al., 2013). The gRNA sequences were generated using the CRISPR Design Tool (Ran et al., 2013; this tool is no longer available). The target sites of the recombination and gRNAs are listed in Table S1.

Gene manipulation

Circular targeting vectors were transfected to mES cells by electroporation using NEPA21 (NepaGene) under the following conditions: poring pulse [voltage: 125 V, pulse length: 5 ms, pulse interval: 50 ms, number of pulses: 2, fading rate: 10%, polarity: +] and transfer pulse [voltage: 20 V, pulse length: 50 ms, pulse interval: 50 ms, number of pulses: 5, fading rate: 40%, polarity: +/−]. Homologous recombination was enhanced by co-transfection of Cas9 nickase expression vectors, which were already cloned with the corresponding gRNAs. Notably, targeting of the *Sox1*, brachyury and *Sox17* genes was performed at a single manipulation to maintain the quality of mES cells. After electroporation, cells recovered in medium without antibiotics for 48 h, and then puromycin selection (1 µg/ml) was started. Culture medium was changed every 2 days for 8-10 days, and the resulting puromycin-resistant colonies were picked and expanded.

Genotyping of homologous recombination

Homologous recombination was confirmed using Southern blotting analysis and a PCR-based genotyping method. For Southern blotting analysis, genomic DNAs were extracted and purified from mES clones, and digested with NheI (*ROSA26* and *Sox1*) or SacI (brachyury and *Sox17*). The digested genomic DNAs were electrophoresed in 0.8% agarose gel, and transferred to positive-charged nitro membranes. The detection of the DNA fragments was performed with DIG-labelled specific probes using PCR DIG Probe Synthetic kit (Roche), which were amplified with the primers listed in Table S2. For genotyping PCR, genomic DNAs were extracted and purified from mES clones or hind limb toes of the infant mice. The specific region of each targeted gene, as shown in Fig. S1, was amplified with PrimeSTAR MAX DNA polymerase (TAKARABIO) using the primers listed in Table S2. PCR amplifications were performed by two-step reaction with 2% DMSO under the following conditions: initial denaturing for 2 min at 98°C, 35 cycles of 10 s at 98°C and 1-5 min at 70°C (*ROSA*, *Sox1*, brachyury and *FLPo*) or 76°C (*Sox17*).

Chimera injection and mice crossing

The homozygous recombinant mES clones were selected and injected into 8-cell embryos derived from ICR mice to produce ROSA reporter mice ($ROSA26^{MultiFPs}$) and triple lineage-labelling mice ($Sox1^{2A\text{-}Cre}$, $Brachyury^{2A\text{-}Dre}$ and $Sox17^{2A\text{-}phiC31o}$). The resultant all F0 chimeric males were crossed with CAG-FLPo (Yamazaki et al., 2016) females to remove puromycin-resistance cassettes flanked by FRTs (*FRT/F3/F5*). $ROSA26^{MultiFPsΔPuro}$ heterozygous F1 mice were inbred to homozygosity, and the resulting homozygous line was maintained. Finally, triple lineage-labelling heterozygous F1 males ($Sox1^{2A\text{-}CreΔPuro/+}$, $Brachyury^{2A\text{-}DreΔPuro/+}$ and $Sox17^{2A\text{-}phiC31oΔPuro/+}$) were crossed with $ROSA26^{MultiFPsΔPuro/MultiFPsΔPuro}$ homozygous females to generate the objective mice. The homozygous $ROSA26^{MultiFPsΔPuro}$ mice and the triple lineage-labelling mice (heterozygous for $Brachyury^{2A\text{-}DreΔPuro}$, homozygous for $Sox1^{2A\text{-}CreΔPuro}$ and $Sox17^{2A\text{-}phiC31oΔPuro}$) will be deposited in the RIKEN BioResource Research Center.

Stereomicroscopic fluorescent imaging of embryos and adult organs

Embryos were dissected from the pregnant females at each time point after crossing. Adult mice were sacrificed at over 8 weeks of age, and all organs were dissected. All surgeries were performed under isoflurane-induced anaesthesia. Embryos and adult organs of mice were observed with fluorescent stereomicroscope system (Olympus, SZX16) with YFP/CFP/RFP2 filters. The contrast of fluorescent image was adjusted to the levels that negative control specimens or backgrounds show minimal auto-fluorescence, using levels tool in Adobe Photoshop CS5, and then the images were merged.

Tissue clearing of embryos

E13.5-E14.5 embryos were fixed with 2% PFA (Nacalai-tesque) in 5% D-sorbitol (Fujifilm Wako)–PHEM buffer [60 mM PIPES (Dojindo), 25 mM HEPES (Sigma), 10 mM EGTA (Dojindo) and 2 mM $MgCl_2$ (Nacalai-tesque), adjusted to pH 8.0] for 2 days at 4°C. After fixation, the samples were washed with PHEM buffer three times. For tissue clearing, the samples were immersed in the permeabilization buffer [PHEM buffer, 2 w/v% saponin (Nacalai-tesque), 5 w/v% D-sorbitol and 0.05 w/v% NaN_3 (Nacalai-tesque)] for over 8 h, and subsequently in a mixture of permeabilization buffer and IMES solution [Omunipaque350 (Daiichi-Sankyo), 2 w/v% saponin, 20 v/v % monoethanolamine (MEA) (Fujifilm Wako), 0.1 v/v% TritonX-100 (Fujifilm Wako), 5 w/v% D-sorbitol, 2.5 mM EDTA (Sigma) and 0.05 w/v% NaN_3] at ratios of 2:1 and 1:1 for 24-48 h, respectively, and then immersed in 100% IMES solution for 24-48 h. All clearing processes were performed at room temperature. Twenty-four hours before imaging, we moved the samples into the mounting solution (Omunipaque350, 0.1% TritonX-100, 5% D-sorbitol, 2.5 mM EDTA and 0.05% NaN_3, adjusted to pH 8.0 and passed through a 0.22 µm pore size filter). Tissue clearing protocols for Sca*l*e U2/S4, SeeDB2 and Ce3D methods have been previously published (Hama et al., 2011, 2015; Ke et al., 2016; Li et al., 2017, respectively). The spatial distributions of the labelled cells were observed on Lightsheet Z.1 microscope (Zeiss) using a 5× objective lens, and excited with 445, 514 and 561 nm lasers for mCerulean, Venus and mCherry, respectively. Images were processed using FIJI (Schindelin et al., 2012), Zen (Zeiss), Vision4D (Arivis) and Imaris (BITPLANE). We stitched the tiled input images and reconstructed the entire stack using Vision4D or Grid/Collection stitching plug-in (Preibisch et al., 2009) in FIJI.

Immunohistochemistry

Adult organs were fixed with the optimal fixative solutions. Brains were fixed with 2% PFA in 5% D-sorbitol–PHEM buffer (pH 8.0) for 2 days at 4°C. Livers and hearts were immersed in ice-cold 5 mM KCl-PHEM buffer (pH 8.0) for 30 min, and then fixed with 0.5% paraformaldehyde in PHEM buffer (pH 8.0) or with the addition of 5% D-sorbitol and 5 mM KCl for 2 days at 4°C. After fixation, the samples were washed with PHEM buffer three times. For vibratome sectioning, the samples were immersed in ice-cold PBS, and sectioned at 300 µm using a VT1200S (Leica) under the following conditions: amplitude 2 mm/s and speed 0.2 mm/s. Tissue slices were permeabilized and blocked in the blocking buffer [1% bovine serum albumin and 2% saponin (brain) or 1% bovine serum albumin, 2% saponin and 0.1-0.3% TritonX-100 (liver and heart) in PHEM buffer (pH 8.0) plus 0.05% NaN_3] over 3 h. Primary and secondary antibodies were diluted in the blocking buffer and incubated for 3 days at room temperature. All staining steps were carried out after 3 washes with the washing buffer [2% saponin (brain) or 2% saponin and 0.1-0.3% TritonX-100 (liver and heart) in PHEM buffer (pH 8.0) plus 0.05% NaN_3]. After secondary antibody washes, the slices were cleared in IMES solution for 20 min, transferred to the mounting solution as described above for 20 min and then mounted on the glass slides in the mounting solution with a 0.3 mm silicon spacer. For frozen sectioning, the heart samples were immersed in 30% sucrose-PHEM buffer

(pH 8.0) for 2 days at 4°C, and then snap-frozen in OCT compound (Sakura-finetek). The frozen samples were cryosectioned at 10 µm using a CM3050S-IV (Leica). The sections were re-hydrated in PHEM buffer for 5 min, and permeabilized and blocked in the blocking buffer as described above, for 20 min. Primary and secondary antibodies were diluted with Can Get Signal solution (TOYOBO) and incubated for 30-60 min at room temperature, respectively. After three washes, the samples were directly mounted in the mounting solution. Confocal microscopy imaging was performed on an inverted LSM880 (Zeiss). Primary and secondary antibodies used in this study are listed in Table S3. Images were processed with FIJI.

Calculation of recombination efficiency in brain endothelial cells

Z-stack images of brain slices (over 200 µm thick) immunostained for PECAM1 were imported into FIJI. The antibody signals (Alexa647 for PECAM-1) and the fluorescent protein signals (mCherry and mCerulean) were processed to threshold images after contrast adjustment with the constant parameter settings. The double-positive (mCherry^{+}/PECAM-1^{+} or mCerulean^{+}/PECAM-1^{+}) pixels were detected using the Calculator Plus plug-in, and the numbers and volumes of the double-positive objects were counted using 3D objects counter plug-in.

Crossreactivity assay in HEK293T cells

ROSA26 reporter plasmid was transfected to HEK293T cells with Lipofectamine 2000 Transfection Reagent (Thermo Fisher Scientific) following the manufacturer's instructions. At 24 h after transfection, the transfected cells were selected with 1 µg/ml puromycin. The resulting drug-resistant cells were passaged, and were advanced to the second transfection of each SSR-expressing plasmid, pCAGGS-Cre, pCAGGS-Dre-ires-puro or pPGKPhiC31obpA. We confirmed the fluorescent signals with the fluorescent microscope system IX81 (Olympus) 6 days after transfections.

Acknowledgements

We thank Doug Sipp for critical reading and revision of the manuscript; A. Francis Stewart for Dre; Philippe Soriano for phiC31o; Dave Piston for mCerulean; Minoru Ko for mCherry; Feng Zhang for CRISPR/Cas9n; Takeshi Yagi for pBTloxP2; Kana Namiki, Tetsushi Hoshida and Atsushi Miyawaki for technical advice; and members of Okano laboratory for discussions. Computational resources were provided by the Data Integration and Analysis Facility, National Institute for Basic Biology, Okazaki, Aichi, Japan.

Competing interests

The authors declare no competing or financial interests.

Author contributions

Conceptualization: T.S., H.O.; Methodology: T.S., A.I., T.M., K.N., S.N., S.S., M.I., H.O.; Validation: A.I., H.O.; Investigation: T.S., A.I., T.M., K.N., S.N., S.S., H.O.; Resources: A.I., S.N., S.S., M.I., H.O.; Data curation: T.S., H.O.; Writing - original draft: T.S., H.O.; Writing - review & editing: T.S., A.I., T.M., K.N., S.N., S.S., M.I., H.O.; Visualization: T.S., S.N.; Supervision: M.I., H.O.; Project administration: T.S., A.I., H.O.; Funding acquisition: S.N., M.I., H.O.

Funding

This research was supported by internal budgets from Keio University, Osaka University and the National Institute for Basic Biology, including the Program for the Advancement of Research in Core Projects on Longevity of the Keio University Global Research Institute from Keio University (to H.O.). This work was also supported by a Japan Society for the Promotion of Science KAKENHI Grant (JP16H06280 to S.N.).

Supplementary information

Supplementary information available online at
http://dev.biologists.org/lookup/doi/10.1242/dev.174938.supplemental

References

Anastassiadis, K., Fu, J., Patsch, C., Hu, S., Weidlich, S., Duerschke, K., Buchholz, F., Edenhofer, F. and Stewart, A. F. (2009). Dre recombinase, like Cre, is a highly efficient site-specific recombinase in E. coli, mammalian cells and mice. *Dis. Model. Mech.* **2**, 508-515. doi:10.1242/dmm.003087

Aramaki, S., Hayashi, K., Kurimoto, K., Ohta, H., Yabuta, Y., Iwanari, H., Mochizuki, Y., Hamakubo, T., Kato, Y., Shirahige, K. et al. (2013). A mesodermal factor, T, specifies mouse germ cell fate by directly activating germline determinants. *Dev. Cell* **27**, 516-529. doi:10.1016/j.devcel.2013.11.001

Becker, K., Jährling, N., Saghafi, S., Weiler, R. and Dodt, H.-U. (2012). Chemical clearing and dehydration of GFP expressing mouse brains. *PLoS ONE* **7**, e33916. doi:10.1371/journal.pone.0033916

Belteki, G., Gertsenstein, M., Ow, D. W. and Nagy, A. (2003). Site-specific cassette exchange and germline transmission with mouse ES cells expressing phiC31 integrase. *Nat. Biotechnol.* **21**, 321-324. doi:10.1038/nbt787

Burtscher, I., Barkey, W., Schwarzfischer, M., Theis, F. J. and Lickert, H. (2012). The Sox17-mCherry fusion mouse line allows visualization of endoderm and vascular endothelial development. *Genesis* **50**, 496-505. doi:10.1002/dvg.20829

Choi, E., Kraus, M. R.-C., Lemaire, L. A., Yoshimoto, M., Vemula, S., Potter, L. A., Manduchi, E., Stoeckert, C. J., Jr., Grapin-Botton, A. and Magnuson, M. A. (2012). Dual lineage-specific expression of Sox17 during mouse embryogenesis. *Stem Cells* **30**, 2297-2308. doi:10.1002/stem.1192

Chung, K., Wallace, J., Kim, S.-Y., Kalyanasundaram, S., Andalman, A. S., Davidson, T. J., Mirzabekov, J. J., Zalocusky, K. A., Mattis, J., Denisin, A. K. et al. (2013). Structural and molecular interrogation of intact biological systems. *Nature* **497**, 332-337. doi:10.1038/nature12107

Dymecki, S. M. (1996). Flp recombinase promotes site-specific DNA recombination in embryonic stem cells and transgenic mice. *Proc. Natl. Acad. Sci. USA* **93**, 6191-6196. doi:10.1073/pnas.93.12.6191

Engert, S., Liao, W. P., Burtscher, I. and Lickert, H. (2009). Sox17-2A-iCre: a knock-in mouse line expressing Cre recombinase in endoderm and vascular endothelial cells. *Genesis* **47**, 603-610. doi:10.1002/dvg.20540

Engert, S., Burtscher, I., Kalali, B., Gerhard, M. and Lickert, H. (2013). The Sox17CreERT2 knock-in mouse line displays spatiotemporal activation of Cre recombinase in distinct Sox17 lineage progenitors. *Genesis* **51**, 793-802. doi:10.1002/dvg.22714

Epelman, S., Lavine, K. J., Beaudin, A. E., Sojka, D. K., Carrero, J. A., Calderon, B., Brija, T., Gautier, E. L., Ivanov, S., Satpathy, A. T. et al. (2014). Embryonic and adult-derived resident cardiac macrophages are maintained through distinct mechanisms at steady state and during inflammation. *Immunity* **40**, 91-104. doi:10.1016/j.immuni.2013.11.019

Frantz, S. and Nahrendorf, M. (2014). Cardiac macrophages and their role in ischaemic heart disease. *Cardiovasc. Res.* **102**, 240-248. doi:10.1093/cvr/cvu025

Groth, A. C., Olivares, E. C., Thyagarajan, B. and Calos, M. P. (2000). A phage integrase directs efficient site-specific integration in human cells. *Proc. Natl. Acad. Sci. USA* **97**, 5995-6000. doi:10.1073/pnas.090527097

Hama, H., Kurokawa, H., Kawano, H., Ando, R., Shimogori, T., Noda, H., Fukami, K., Sakaue-Sawano, A. and Miyawaki, A. (2011). Scale: a chemical approach for fluorescence imaging and reconstruction of transparent mouse brain. *Nat. Neurosci.* **14**, 1481-1488. doi:10.1038/nn.2928

Hama, H., Hioki, H., Namiki, K., Hoshida, T., Kurokawa, H., Ishidate, F., Kaneko, T., Akagi, T., Saito, T., Saido, T. et al. (2015). ScaleS: an optical clearing palette for biological imaging. *Nat. Neurosci.* **18**, 1518-1529. doi:10.1038/nn.4107

Hoeffel, G., Chen, J., Lavin, Y., Low, D., Almeida, F. F., See, P., Beaudin, A. E., Lum, J., Low, I., Forsberg, E. C. et al. (2015). C-Myb(+) erythro-myeloid progenitor-derived fetal monocytes give rise to adult tissue-resident macrophages. *Immunity* **42**, 665-678. doi:10.1016/j.immuni.2015.03.011

Hu, X., Li, P., Guo, Y., Wang, H., Leak, R. K., Chen, S., Gao, Y. and Chen, J. (2012). Microglia/macrophage polarization dynamics reveal novel mechanism of injury expansion after focal cerebral ischemia. *Stroke* **43**, 3063-3070. doi:10.1161/STROKEAHA.112.659656

Kamachi, Y., Uchikawa, M., Collignon, J., Lovell-Badge, R. and Kondoh, H. (1998). Involvement of Sox1, 2 and 3 in the early and subsequent molecular events of lens induction. *Development* **125**, 2521-2532.

Kanazawa, M., Miura, M., Toriyabe, M., Koyama, M., Hatakeyama, M., Ishikawa, M., Nakajima, T., Onodera, O., Takahashi, T., Nishizawa, M. et al. (2017). Microglia preconditioned by oxygen-glucose deprivation promote functional recovery in ischemic rats. *Sci. Rep.* **7**, 42582. doi:10.1038/srep42582

Karimova, M., Abi-Ghanem, J., Berger, N., Surendranath, V., Pisabarro, M. T. and Buchholz, F. (2013). Vika/vox, a novel efficient and specific Cre/loxP-like site-specific recombination system. *Nucleic Acids Res.* **41**, e37. doi:10.1093/nar/gks1037

Karimova, M., Splith, V., Karpinski, J., Pisabarro, M. T. and Buchholz, F. (2016). Discovery of Nigri/nox and Panto/pox site-specific recombinase systems facilitates advanced genome engineering. *Sci. Rep.* **6**, 30130. doi:10.1038/srep30130

Ke, M.-T., Fujimoto, S. and Imai, T. (2013). SeeDB: a simple and morphology-preserving optical clearing agent for neuronal circuit reconstruction. *Nat. Neurosci.* **16**, 1154-1161. doi:10.1038/nn.3447

Ke, M.-T., Nakai, Y., Fujimoto, S., Takayama, R., Yoshida, S., Kitajima, T. S., Sato, M. and Imai, T. (2016). Super-resolution mapping of neuronal circuitry with an index-optimized clearing agent. *Cell Rep.* **14**, 2718-2732. doi:10.1016/j.celrep.2016.02.057

Kierdorf, K., Erny, D., Goldmann, T., Sander, V., Schulz, C., Perdiguero, E. G., Wieghofer, P., Heinrich, A., Riemke, P., Hölscher, C. et al. (2013). Microglia

emerge from erythromyeloid precursors via Pu.1- and Irf8-dependent pathways. *Nat. Neurosci.* **16**, 273-280. doi:10.1038/nn.3318

Kim, J. H., Lee, S.-R., Li, L.-H., Park, H.-J., Park, J.-H., Lee, K. Y., Kim, M.-K., Shin, B. A. and Choi, S.-Y. (2011). High cleavage efficiency of a 2A peptide derived from porcine teschovirus-1 in human cell lines, zebrafish and mice. *PLoS ONE* **6**, e18556. doi:10.1371/journal.pone.0018556

Kohyama, J., Tokunaga, A., Fujita, Y., Miyoshi, H., Nagai, T., Miyawaki, A., Nakao, K., Matsuzaki, Y. and Okano, H. (2005). Visualization of spatiotemporal activation of Notch signaling: live monitoring and significance in neural development. *Dev. Biol.* **286**, 311-325. doi:10.1016/j.ydbio.2005.08.003

Kumar, A., Lualdi, M., Lewandoski, M. and Kuehn, M. R. (2008). Broad mesodermal and endodermal deletion of Nodal at postgastrulation stages results solely in left/right axial defects. *Dev. Dyn.* **237**, 3591-3601. doi:10.1002/dvdy.21665

Li, W., Germain, R. N. and Gerner, M. Y. (2017). Multiplex, quantitative cellular analysis in large tissue volumes with clearing-enhanced 3D microscopy (C_e3D). *Proc. Natl. Acad. Sci. USA* **114**, E7321-E7330. doi:10.1073/pnas.1708981114

Liao, W. P., Uetzmann, L., Burtscher, I. and Lickert, H. (2009). Generation of a mouse line expressing Sox17-driven Cre recombinase with specific activity in arteries. *Genesis* **47**, 476-483. doi:10.1002/dvg.20520

Liu, Z., Chen, O., Wall, J. B. J., Zheng, M., Zhou, Y., Wang, L., Ruth Vaseghi, H., Qian, L. and Liu, J. (2017). Systematic comparison of 2A peptides for cloning multi-genes in a polycistronic vector. *Sci. Rep.* **7**, 2193. doi:10.1038/s41598-017-02460-2

Liu, K., Yu, W., Tang, M., Tang, J., Liu, X., Liu, Q., Li, Y., He, L., Zhang, L., Evans, S. M. et al. (2018). A dual genetic tracing system identifies diverse and dynamic origins of cardiac valve mesenchyme. *Development* **145**, dev167775. doi:10.1242/dev.167775

Luke, G. A., de Felipe, P., Lukashev, A., Kallioinen, S. E., Bruno, E. A. and Ryan, M. D. (2008). Occurrence, function and evolutionary origins of '2A-like' sequences in virus genomes. *J. Gen. Virol.* **89**, 1036-1042. doi:10.1099/vir.0.83428-0

Mabuchi, T., Kitagawa, K., Ohtsuki, T., Kuwabara, K., Yagita, Y., Yanagihara, T., Hori, M. and Matsumoto, M. (2000). Contribution of microglia/macrophages to expansion of infarction and response of oligodendrocytes after focal cerebral ischemia in rats. *Stroke* **31**, 1735-1743. doi:10.1161/01.STR.31.7.1735

McLeod, M., Craft, S. and Broach, J. R. (1986). Identification of the crossover site during FLP-mediated recombination in the Saccharomyces cerevisiae plasmid 2 microns circle. *Mol. Cell. Biol.* **6**, 3357-3367. doi:10.1128/MCB.6.10.3357

Nagai, T., Ibata, K., Park, E. S., Kubota, M., Mikoshiba, K. and Miyawaki, A. (2002). A variant of yellow fluorescent protein with fast and efficient maturation for cell-biological applications. *Nat. Biotechnol.* **20**, 87-90. doi:10.1038/nbt0102-87

Nishiguchi, S., Wood, H., Kondoh, H., Lovell-Badge, R. and Episkopou, V. (1998). Sox1 directly regulates the gamma-crystallin genes and is essential for lens development in mice. *Genes Dev.* **12**, 776-781. doi:10.1101/gad.12.6.776

Ogawa, K., Nishinakamura, R., Iwamatsu, Y., Shimosato, D. and Niwa, H. (2006). Synergistic action of Wnt and LIF in maintaining pluripotency of mouse ES cells. *Biochem. Biophys. Res. Commun.* **343**, 159-166. doi:10.1016/j.bbrc.2006.02.127

Orban, P. C., Chui, D. and Marth, J. D. (1992). Tissue- and site-specific DNA recombination in transgenic mice. *Proc. Natl. Acad. Sci. USA* **89**, 6861-6865. doi:10.1073/pnas.89.15.6861

Ormel, P. R., Vieira de Sá, R., van Bodegraven, E. J., Karst, H., Harschnitz, O., Sneeboer, M. A. M., Johansen, L. E., van Dijk, . R. E., Scheefhals, N., Berdenis van Berlekom, A. et al. (2018). Microglia innately develop within cerebral organoids. *Nat. Commun.* **9**, 4167. doi:10.1038/s41467-018-06684-2

Pennimpede, T., Proske, J., König, A., Vidigal, J. A., Morkel, M., Bramsen, J. B., Herrmann, B. G. and Wittler, L. (2012). In vivo knockdown of Brachyury results in skeletal defects and urorectal malformations resembling caudal regression syndrome. *Dev. Biol.* **372**, 55-67. doi:10.1016/j.ydbio.2012.09.003

Perantoni, A. O., Timofeeva, O., Naillat, F., Richman, C., Pajni-Underwood, S., Wilson, C., Vainio, S., Dove, L. F. and Lewandoski, M. (2005). Inactivation of FGF8 in early mesoderm reveals an essential role in kidney development. *Development* **132**, 3859-3871. doi:10.1242/dev.01945

Perego, C., Fumagalli, S. and De Simoni, M.-G. (2011). Temporal pattern of expression and colocalization of microglia/macrophage phenotype markers following brain ischemic injury in mice. *J. Neuroinflammation* **8**, 174. doi:10.1186/1742-2094-8-174

Preibisch, S., Saalfeld, S. and Tomancak, P. (2009). Globally optimal stitching of tiled 3D microscopic image acquisitions. *Bioinformatics* **25**, 1463-1465. doi:10.1093/bioinformatics/btp184

Ran, F. A., Hsu, P. D., Wright, J., Agarwala, V., Scott, D. A. and Zhang, F. (2013). Genome engineering using the CRISPR-Cas9 system. *Nat. Protoc.* **8**, 2281-2308. doi:10.1038/nprot.2013.143

Raymond, C. S. and Soriano, P. (2007). High-efficiency FLP and PhiC31 site-specific recombination in mammalian cells. *PLoS ONE* **2**, e162. doi:10.1371/journal.pone.0000162

Rizzo, M. A., Springer, G. H., Granada, B. and Piston, D. W. (2004). An improved cyan fluorescent protein variant useful for FRET. *Nat. Biotechnol.* **22**, 445-449. doi:10.1038/nbt945

Sauer, B. and Henderson, N. (1988). Site-specific DNA recombination in mammalian cells by the Cre recombinase of bacteriophage P1. *Proc. Natl. Acad. Sci. USA* **85**, 5166-5170. doi:10.1073/pnas.85.14.5166

Schindelin, J., Arganda-Carreras, I., Frise, E., Kaynig, V., Longair, M., Pietzsch, T., Preibisch, S., Rueden, C., Saalfeld, S., Schmid, B. et al. (2012). Fiji: an open-source platform for biological-image analysis. *Nat. Methods* **9**, 676-682. doi:10.1038/nmeth.2019

Schlake, T. and Bode, J. (1994). Use of mutated FLP recognition target (FRT) sites for the exchange of expression cassettes at defined chromosomal loci. *Biochemistry* **33**, 12746-12751. doi:10.1021/bi00209a003

Sternberg, N. and Hamilton, D. (1981). Bacteriophage P1 site-specific recombination. I. *J. Mol. Biol.* **150**, 467-486. doi:10.1016/0022-2836(81)90375-2

Sternberg, N., Hamilton, D. and Hoess, R. (1981). Bacteriophage P1 site-specific recombination. II. *J. Mol. Biol.* **150**, 487-507. doi:10.1016/0022-2836(81)90376-4

Susaki, E. A., Tainaka, K., Perrin, D., Kishino, F., Tawara, T., Watanabe, T. M., Yokoyama, C., Onoe, H., Eguchi, M., Yamaguchi, S. et al. (2014). Whole-brain imaging with single-cell resolution using chemical cocktails and computational analysis. *Cell* **157**, 726-739. doi:10.1016/j.cell.2014.03.042

Suzuki, E. and Nakayama, M. (2011). VCre/VloxP and SCre/SloxP: new site-specific recombination systems for genome engineering. *Nucleic. Acids Res.* **39**, e49. doi:10.1093/nar/gkq1280

Takashima, Y., Era, T., Nakao, K., Kondo, S., Kasuga, M., Smith, A. G. and Nishikawa, S.-I. (2007). Neuroepithelial cells supply an initial transient wave of MSC differentiation. *Cell* **129**, 1377-1388. doi:10.1016/j.cell.2007.04.028

Takemoto, T., Uchikawa, M., Yoshida, M., Bell, D. M., Lovell-Badge, R., Papaioannou, V. E. and Kondoh, H. (2011). Tbx6-dependent Sox2 regulation determines neural or mesodermal fate in axial stem cells. *Nature* **470**, 394-398. doi:10.1038/nature09729

Tanimoto, Y., Iijima, S., Hasegawa, Y., Suzuki, Y., Daitoku, Y., Mizuno, S., Ishige, T., Kudo, T., Takahashi, S., Kunita, S. et al. (2008). Embryonic stem cells derived from C57BL/6J and C57BL/6N mice. *Comp. Med.* **58**, 347-352.

Treweek, J. B., Chan, K. Y., Flytzanis, N. C., Yang, B., Deverman, B. E., Greenbaum, A., Lignell, A., Xiao, C., Cai, L., Ladinsky, M. S. et al. (2015). Whole-body tissue stabilization and selective extractions via tissue-hydrogel hybrids for high-resolution intact circuit mapping and phenotyping. *Nat. Protoc.* **10**, 1860-1896. doi:10.1038/nprot.2015.122

Yamazaki, D., Miyata, H., Funato, Y., Fujihara, Y., Ikawa, M. and Miki, H. (2016). The Mg2+ transporter CNNM4 regulates sperm Ca2+ homeostasis and is essential for reproduction. *J. Cell Sci.* **129**, 1940-1949. doi:10.1242/jcs.182220

Ying, Q.-L., Stavridis, M., Griffiths, D., Li, M. and Smith, A. (2003). Conversion of embryonic stem cells into neuroectodermal precursors in adherent monoculture. *Nat. Biotechnol.* **21**, 183-186. doi:10.1038/nbt780

Yokota, S., Hirayama, T., Hirano, K., Kaneko, R., Toyoda, S., Kawamura, Y., Hirabayashi, M., Hirabayashi, T. and Yagi, T. (2011). Identification of the cluster control region for the Protocadherin-β genes located beyond the Protocadherin-γ cluster. *J. Biol. Chem.* **286**, 31885-31895. doi:10.1074/jbc.M111.245605

Zong, H., Espinosa, J. S., Su, H. H., Muzumdar, M. D. and Luo, L. (2005). Mosaic analysis with double markers in mice. *Cell* **121**, 479-492. doi:10.1016/j.cell.2005.02.012

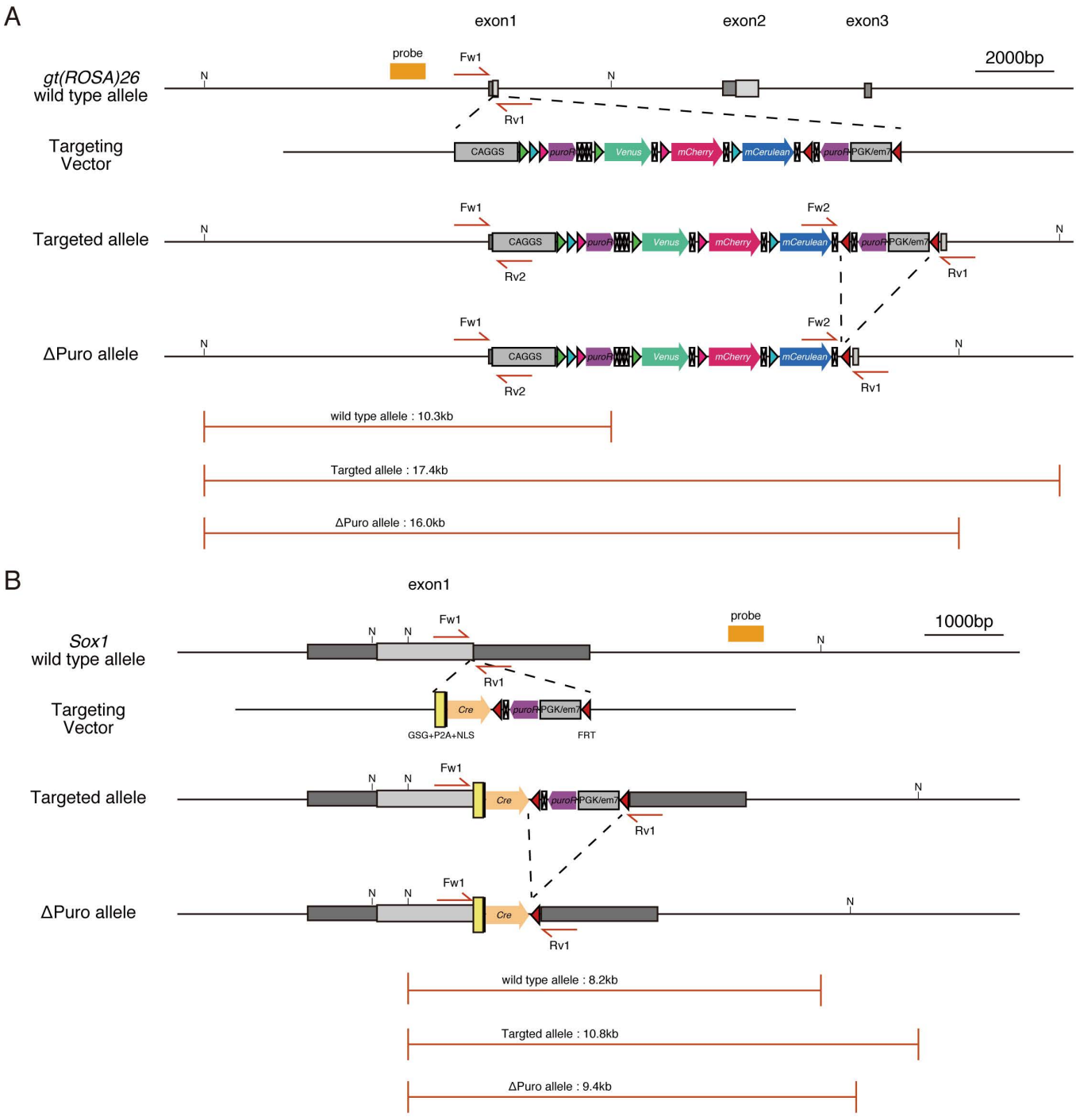

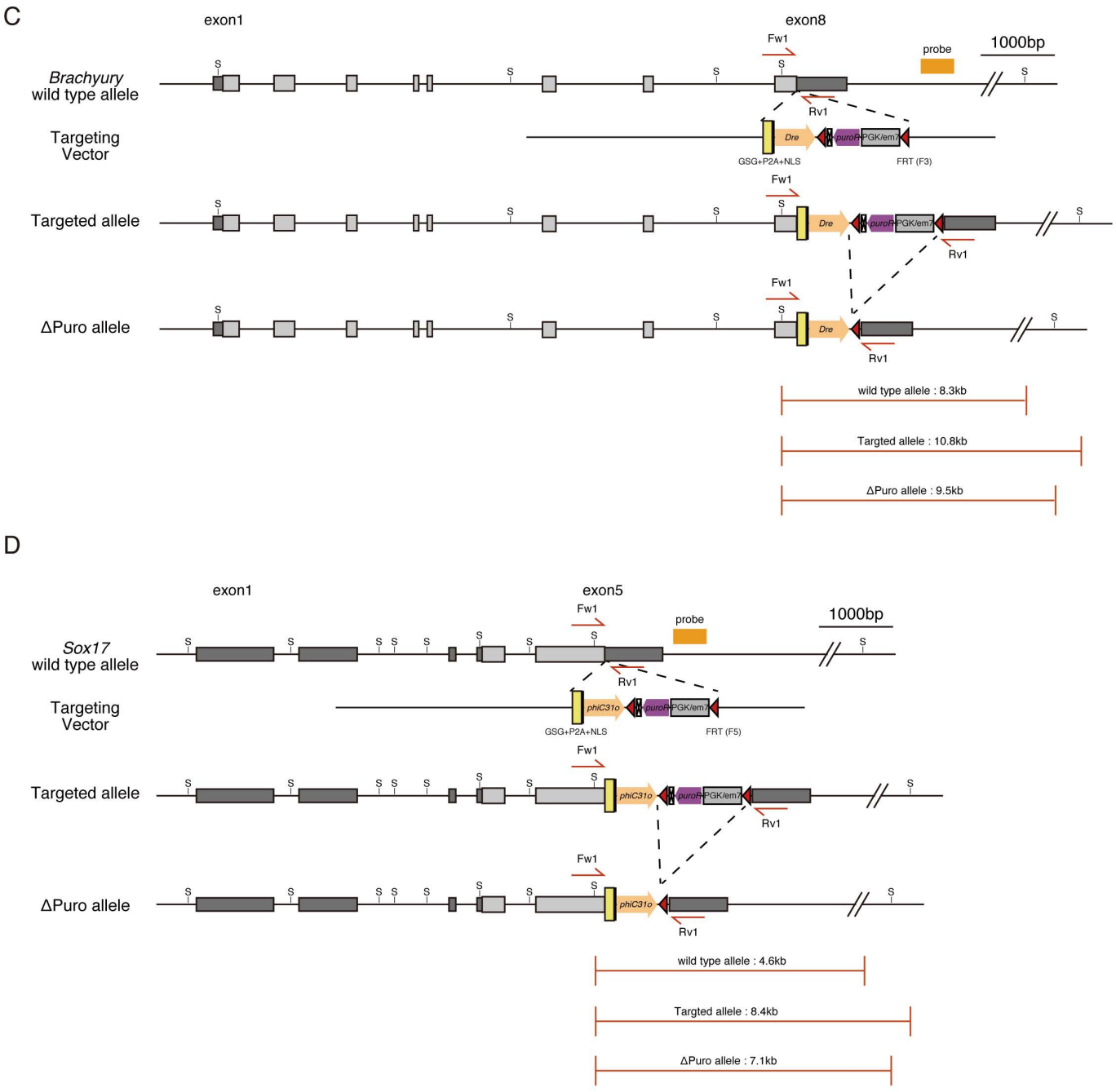

Fig. S1. Detailed targeting strategies and generation of the *TRiCK* system.

(A-D) Targeting alleles of *Gt(ROSA)26* locus for *ROSA*^{MultiFPsΔPuro} (A), *Sox1* locus for *Sox1*$^{2A\text{-}CreΔPuro}$ (B), *Brachyury* (*T*) locus for *Brachyury*$^{2A\text{-}DreΔPuro}$ (C), and *Sox17* locus for *Sox17*$^{2A\text{-}phiC31oΔPuro}$ (D), respectively. (E) Genomic PCR result for *ROSA*^{MultiFPs} alleles. (F) Southern blotting analyses for *Sox1*$^{2A\text{-}Cre}$, *Brachyury*$^{2A\text{-}Dre}$, and *Sox17*$^{2A\text{-}phiC31o}$ alleles.

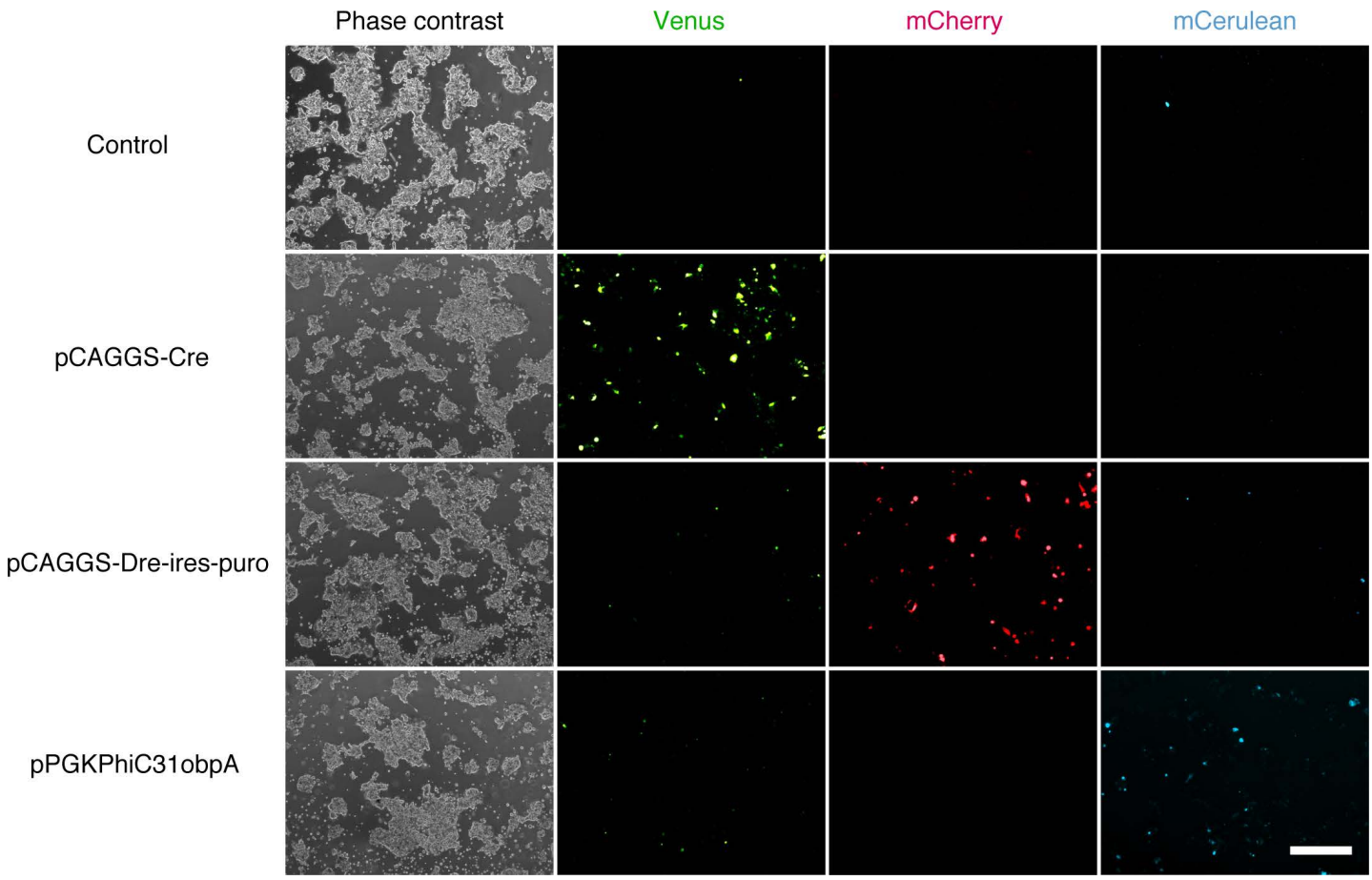

Fig. S2. Confirmation of the properties of site-specific recombinases *in vitro*.

We transfected the reporter plasmid to HEK293T cell. The stable puromycin-resistant transfectant was subsequently transfected with the SSR-expressing plasmids and analysed for fluorescent protein expressions. The transfectant without SSR-expressing plasmid was used as the control. Each SSR did not show any cross-reactivity, however, mCerulean/*att* system showed relatively low recombination efficiency compared with Cre/*loxP* and Dre/*rox* systems. Scale bar: 500 μm. Representative images of two independent experiments are presented.

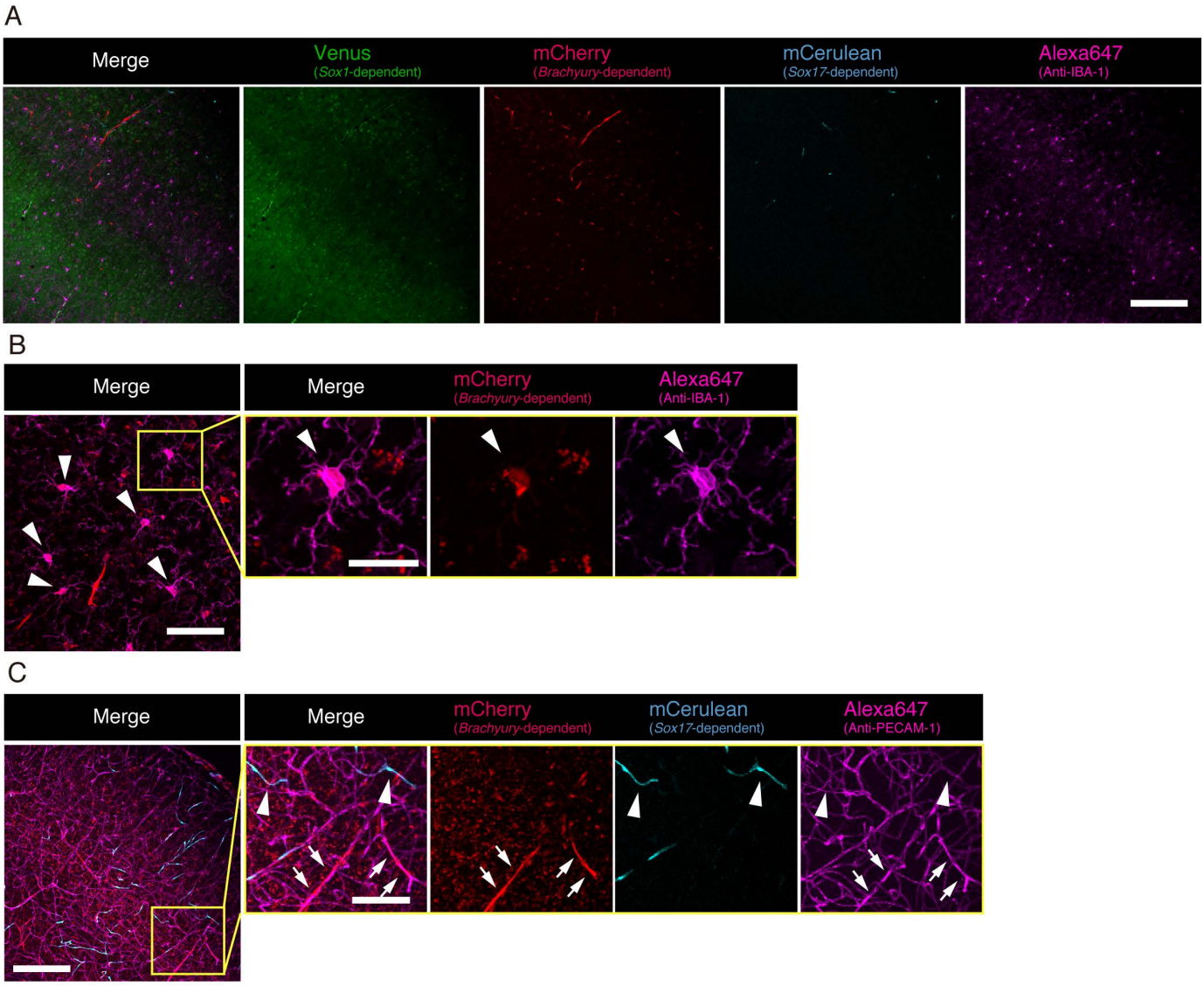

Fig. S3. Specific cell types were identified with immunostaining in the adult *TRiCK* mouse brain.

To specify the cell types of the labelled cells in the adult *TRiCK* mouse brain, we performed immunostaining with cell type-specific markers. (A, B) Almost all mCherry+ cells in brain were also stained with IBA-1 (arrowheads), a microglial marker, depicting their glia processes. (C) Staining for an endothelial marker PECAM-1 demonstrated the PECAM-1+ capillary endothelial cells had either mCherry+ (arrows) or mCerulean+ (arrowheads) phenotypes. Z-stack images were processed to a single plane by imaging software in B and C. *Sox1*$^{2A\text{-}Cre\Delta Puro}$ drove Venus (green); *Brachyury*$^{2A\text{-}Dre\Delta Puro}$ drove mCherry (red); *Sox17*$^{2A\text{-}phiC31o\Delta Puro}$ drove mCerulean (cyan). Scale bars: 200 μm in A, C; 50 μm in B (20 μm in inset). Representative images of three individual biological specimens are presented.

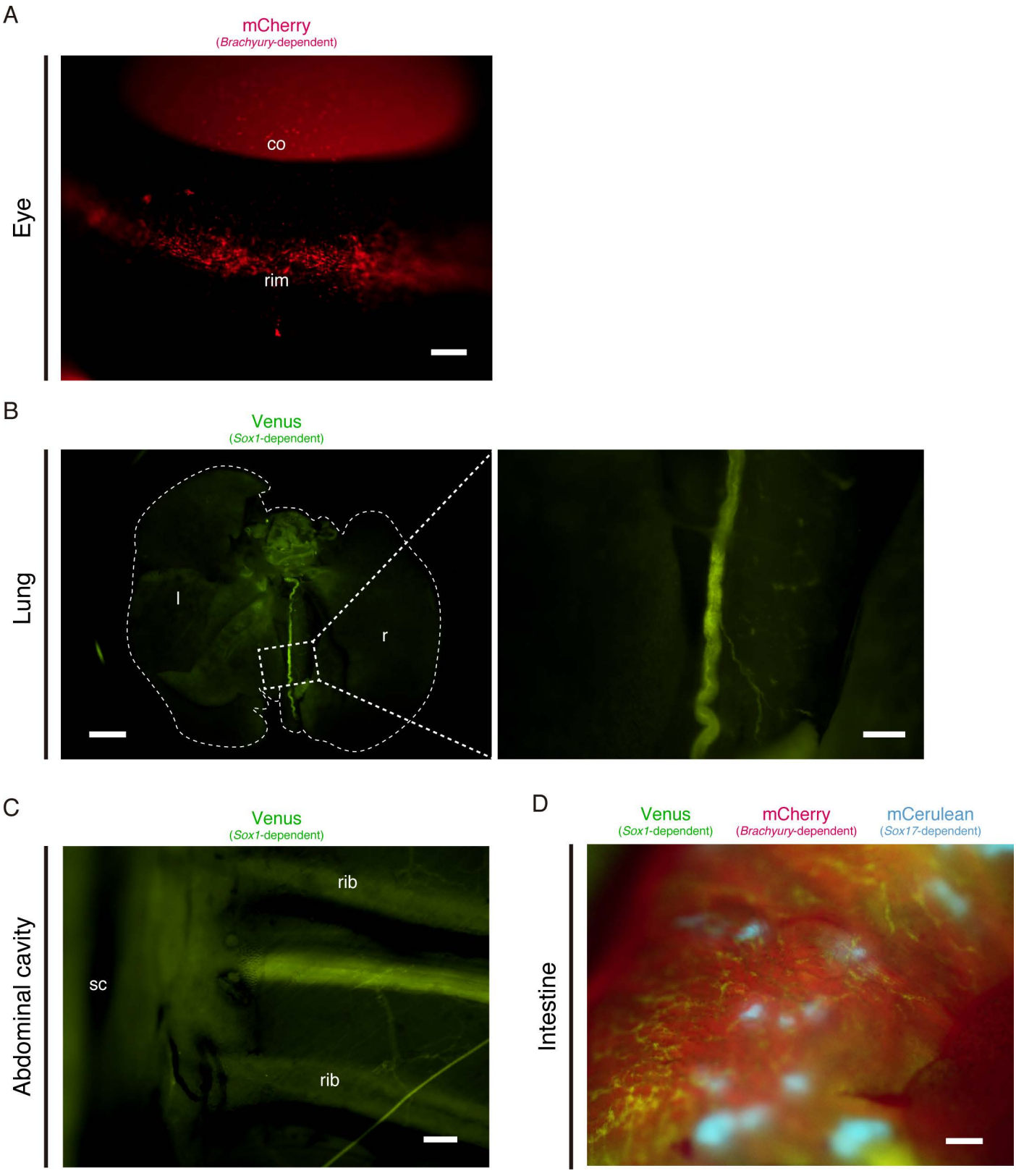

Fig. S4. High magnification stereoscopic observations on adult TRiCK mouse organs.

The high magnified images of the eyes, lung, abdominal cavity, and intestines of the specimens as shown in Figure 4 are presented. (A) mCherry+ mesodermal cells were distributed in the cornea stroma and resided at the connective tissues of the eye rim (rim). co, cornea. (B) We observed Venus+ peripheral nerves extended on the trachea on the dorsal side of the lung. l, left lung; r, right lung. (C) The periheral nerves could be labelled with Venus in thoracic domain, which are detectable from the abdominal cavity. sc, spinal column; rib, ribs. (D) The enteric nervous system was distinctly visualized with Venus. *Sox1*$^{2A\text{-}Cre\Delta Puro}$ drove Venus (green); *Brachyury*$^{2A\text{-}Dre\Delta Puro}$ drove mCherry (red); *Sox17*$^{2A\text{-}phiC31o\Delta Puro}$ drove mCerulean (cyan). Scale bars: 200 μm in A, C, D; 1 mm in B (200 μm in the magnified view). Representative images of five individual biological specimens are presented.

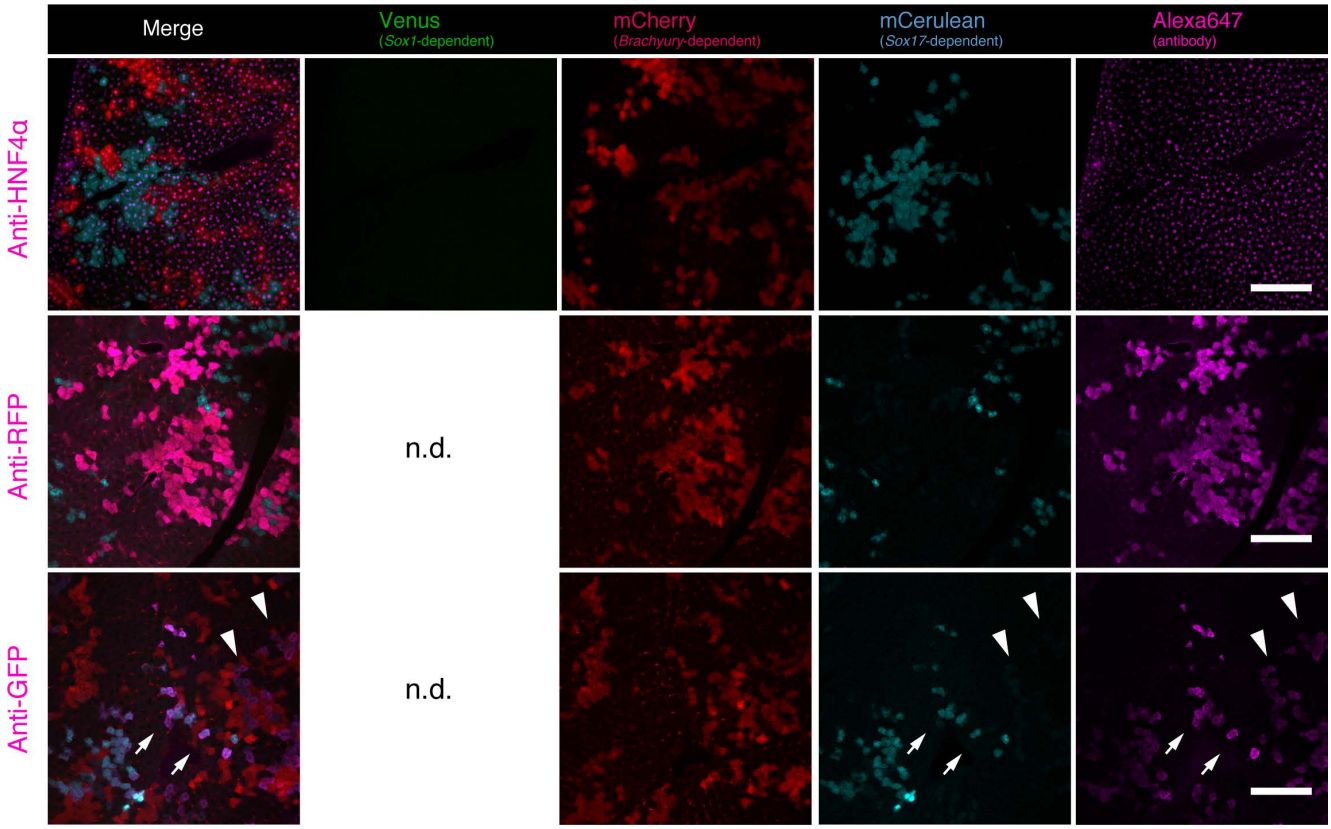

Fig. S5. Immunohistological validation for lineage labels in *TRiCK* mouse liver.

Cellular types of the lineage labelled cells in the liver were identified with immunohistochemistry on vibratome sections. Immunostained results for anti-HNF4α (upper), anti-RFP (middle), and anti-GFP (bottom). Arrows in bottom images indicate mCelurean+/anti-GFP+ cells, and arrowheads in the same indicate mCelurean(-) or mCerulean(weak)/anti-GFP+ cells. *Sox1*$^{2A\text{-}Cre\Delta Puro}$ drove Venus (green); *Brachyury*$^{2A\text{-}Dre\Delta Puro}$ drove mCherry (red); *Sox17*$^{2A\text{-}phiC31o\Delta Puro}$ drove mCerulean (cyan). Scale bars: 200 μm; n.d., no data. Representative images of three individual biological specimens are presented.

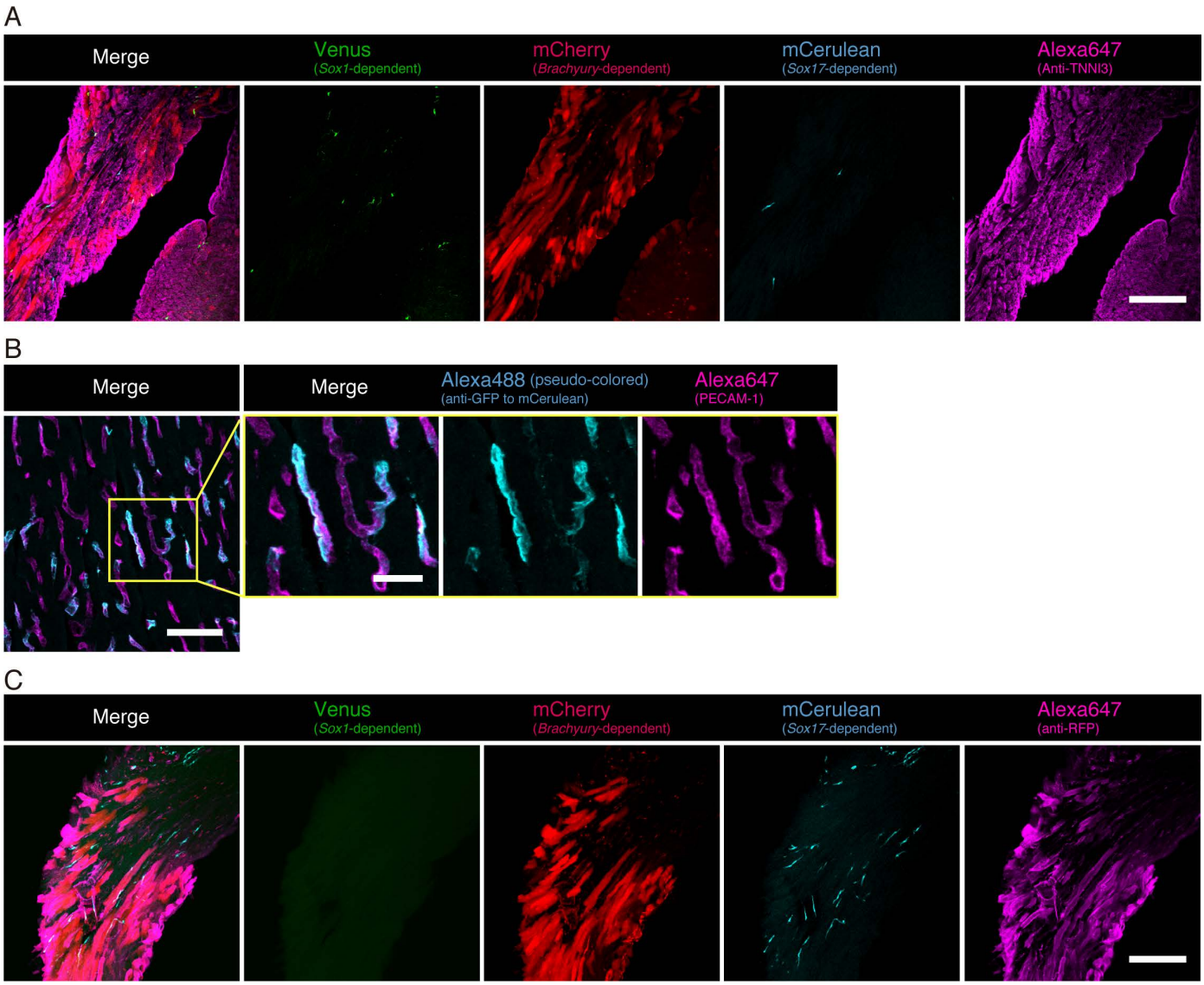

Fig. S6. Immunohistological validation for lineage labels in *TRiCK* mouse heart.

We performed immunolabelling on vibratome section (A, C) or frozen section (B) to characterize cell types of mCherry+ cells and mCerulean+ cells in the heart. Immunostained images for a cardiomyocyte marker TNNI3 (A), an endothelial marker PECAM-1 (B), and RFP (C). The signal of anti-GFP enhanced by second antibody conjugated with Alexa488 was visualized in pseudo-coloured cyan. Z-stack images were processed to a single plane by imaging software in A–C. *Sox1*$^{2A\text{-}Cre\Delta Puro}$ drove Venus (green); *Brachyury*$^{2A\text{-}Dre\Delta Puro}$ drove mCherry (red); *Sox17*$^{2A\text{-}phiC31o\Delta Puro}$ drove mCerulean (cyan). Scale bars: 200 µm in A, C; 50 µm in B (20 µm in inset). Representative images of three individual biological specimens are presented.

Table S1. Target sites of recombinations and gRNA sequences.

Constructions	Methods	Names	sequence (5′→3′)	(bp)
ROSA^{MultiFPs}	BAC recombination	5′ arm	CGGGGCCGCCTAAAGAAGAGGCTGTGCTTTGGGGC TCC	38
		3′ arm	GGCGGCCGCGGCAGGCCCTCCGAGCGTGGTGGAG CCGT	38
	BAC retrieval	5′ arm	GTAGACCAGGCTGGCCTCGAACTCAGAAATCCGCCT GCCTCTGCCTCCTGAGTGCCGGGATTAAAGGCGTGC ACCACCACGCCTGGCTAAGTTGGATATTTTGTTATATA ACTATAACCAATACTAACTCCACTGGGTGGATTTTTAA TTCAGTCAGTAGTCTTAAGTGGTCTTTATTGGCCCTTC ATTAAAATCTACTGTTCACTCTAACAGAGGCTGTTGGT ACTAGTGGCACTTAAGCAACTTCCTACGG	253
		3′ arm	CAACACTGCCTCCCTGCTGTGCAAAGAGCCCTTTGT CCTGCCCCGCACTTATCTAGCTGTTTGGCCATATTGA CAGGCCTACTGGAGGCATAATAAGGGAGTCAGTCTG ACATAAGCAGCTGGCGATTTCAAACAAAAATCTTCCTT TTCTACTCACACAAAATCCTGCTGCAGAGGTCTGTGG CTCCTCCCATACTTCCACCTAGTTCTCAAATAGAGCA GCAAGGAACTGGCATTTCC	240
	gRNA	sgRNA1	CCCGATCCCCTACCTAGCCG AGG	23
		sgRNA2	GGGCGGCTTGGTGCGTTTGC GGG	23
Sox1$^{2A\text{-}Cre}$	BAC recombination	5′ arm	CAGCACTACCAGGGCGCGGGCGCGGGCGTCAACGG CACGGTGCCCCTGACGCACATC	57
		3′ arm	CGCCGCGGGGACGCCGGGGACACTGCGGCTTAAGG CCGGCGCCCCGGCGACG	52
	BAC retrieval	5′ arm	GCTAAGTGACCTTCTGGGGAAATTTGCCTGTGTCAGA GACGGTGGCCTTAGAGTCTTCCTGAATGCCCTGCGG ATTTCTCGTGAG	85
		3′ arm	GAGGTCTGGCACACCATGCCCACCACTGCTTAGTTG GCACAGACTGCAACCACCAATCTTCTCTGTCACTTGG CAACAGGTTAC	84
	gRNA	sgRNA1	CGCGGCGCTAGATGTGCGTC AGG	23
		sgRNA2	GCGGCTTAAGGCCGGCGCCC CGG	23
Brachyury$^{2A\text{-}Dre}$	BAC recombination	5' arm	GACACGGCCCAAAGCCTCCTCATAGCCTCGTGGACA CCTGTGTCACCCCCATCTATG	57
		3' arm	ATTGAACTTTCCTCCATGTGCTGAGACTTGTAACAAC CGGTGTCAACTGGATC	53
	BAC retrieval	5' arm	GATGGTGTGTGTGTGCCTGTGTGTACCTGGATATATAT CCCTGTGTATACATAATAGTTTACATATGGGAGCCATA CTCCTAGG	84
		3' arm	GCATAAACCACAACTTCACGGTTTTAAGATCTGGAGA GGAGAGGGGACAGCTCTTGATCTCAGCAACGGGAAA GTCCTGGCA	82
	gRNA	sgRNA1	AGTTCAATTCACATAGATGG GGG	23
		sgRNA2	TTGTAACAACCGGTGTCAAC TGG	23

Table S1. Target sites of recombinations and gRNA sequences. (*continued from previous page*)

Constructions	Methods	Names	sequence (5′→3′)	(bp)
Sox17$^{2A\text{-}phiC31o}$	BAC recombination	5′ arm	GGATCCTGGCGCCCCCCAGCGCTCTGCACCTGTACT ACGGCGCGATGGGCTCGCCCGCCGCAAGTGCGGGG CGCGGTTTCCACGCGCAACCCCAGCAGCCGCTGCA ACCGCAGGCACCGCCGCCGCCACCGCAGCAGCAGC ACCCAGCGCACGGCCCCGGGCAACCTTCGCCCCCT CCCGAGGCTCTGCCCTGCCGGGATGGCACGGAATC CAACCAGCCCACTGAGCTCCTAGGGGAGGTGGACC GCACGGAATTCGAACAGTATCTGCCCTTTGTGTATAA GCCCGAGATGGGTCTTCCCTACCAGGGACACGACTG CGGAGTGAACCTCTCAGACAGCCACGGAGCCATTTC CTCCGTGGTGTCCGACGCTAGCTCAGCGGTCTACTA TTGCAACTACCCCGACATT	410
		3′ arm	CGGTTGCCGACCCGACCTGAGGGCCAGAAGCAGTG TTACACACTTCCTGGAAGCG	55
	BAC retrieval	5′ arm	ACCGGTTACTGAGCTGGGAAGTGGAGCGGGAGCAG TTTACTTCCTGCTTCGCCGCGGAAAAACTCAGCTAGG GCCGAGCGGGAAGGAGG	89
		3′ arm	TTTGTTATGAGTCACATGATTCACATGATTTAACTAACA GATACTATTCTCTTGAATTTAAAGGGAGCCTATAATGTA TGGTGAGATGAAGATG	94
	gRNA	sgRNA1	GTAGACCGCTGAGCTAGCGT CGG	23
		sgRNA2	GCAACTACCCCGACATTTGA CGG	23

Table S2. Primers used in this study.

Alleles	Methods	Names	sequence (5′→3′)	(bp)
ROSA^{MultiFPs}	Genotyping PCR	Fw1	GCACTACTGTGTTGGCGGACTGG	23
		Fw2	GTGCCTTCTAGTTGCCAGCCATCTGT	26
		Rv1	TCGTACCCGGCTGTCTCACAGAAC	24
		Rv2	GATGGGGAGAGTGAAGCAGAACGTGG	26
	Southern blotting probe	Fw	GAGCACAGGAACAATTGGCAAAAGG	25
		Rv	CTCCATAATCTTCCTGAACGCCTCTC	26
		probe	(-)	627
Sox1^{2A-Cre}	Genotyping PCR	Fw1	CCCTCGGATCTCTGGTCAAGTCGGA	25
		Rv1	GCTCTCCAGAGCGGCCTTTTATCGAGA	27
	Southern blotting probe	Fw	GAAGGCCGTTGGGGAATTAAGAAAAG	26
		Rv	CTGTCTTAGTAATGCCTTCCGTTCAATAC	29
		probe	(-)	628
Brachyury^{2A-Dre}	Genotyping PCR	Fw1	CTTTCGAGGCTCCCCTGCACATTACAC	27
		Rv1	CTAAGGCAACAAGGGAGGACATTAGAGGTG	30
	Southern blotting probe	Fw	GTGTAATTTGCATCCATTTCTGAGAGG	27
		Rv	GTGGATGAAGGAAGATTGTTGTACTCAA	28
		probe	(-)	606
Sox17$^{2A-phiC31o}$	Genotyping PCR	Fw1	ACGGAATCCAACCAGCCCACTGAGC	25
		Rv1	AACACTGCTTCTGGCCCTCAGGTC	24
	Southern blotting probe	Fw	GCTATAGCTAGATTGTGTCCCTTCA	25
		Rv	GCTCAACCTTTTGTCACTGAAAATGTC	27
		probe	(-)	606
FLPo	Genotyping PCR	Fw1	GCAACGTGCTGGTTGTTGTGCTGTCTCATC	30
		Rv1	ACTCGAGTCAGACCGCCTGTTGATGTAGCTG	31

Table S3. Antibody list in this study			
Designation	Source	Identifiers	Dilution
Rabbit polyclonal anti-Iba1	Fujifilm Wako	019-19741	1:200
Rat monoclonal anti-CD31 (PECAM-1)	BD Bioscience	553370	1:500
Goat polyclonal anti-Cardiac Troponin I (TNNI3)	Abcam	ab56357	1:200
Mouse monoclonal anti-HNF4α	Perseus Proteomics	PP-H1415-00	1:100
Chick polyclonal anti-GFP	Aves Lab	GFP-1010	1:1000
Rabbit polyclonal anti-RFP	MBL	PM005	1:200
Rat monoclonal anti-CD11b	BioLegend	101201	1:200
Rat monoclonal anti-F4/80	Abcam	ab6640	1:200
Goat anti-rabbit IgG Alexa647 conjugate	Thermo fisher scientific	A21245	1:500
Goat anti-rat IgG Alexa647 conjugate	Thermo fisher scientific	A21247	1:500
Goat anti-mouse IgG2a Alexa647 conjugate	Thermo fisher scientific	A21241	1:500
Goat anti-chick IgY Alexa647 conjugate	Thermo fisher scientific	A21449	1:500
Goat anti-chick IgY Alexa488 conjugate	Thermo fisher scientific	A11039	1:500
Donkey anti-goat IgG Alexa647 conjugate	Thermo fisher scientific	A21447	1:500

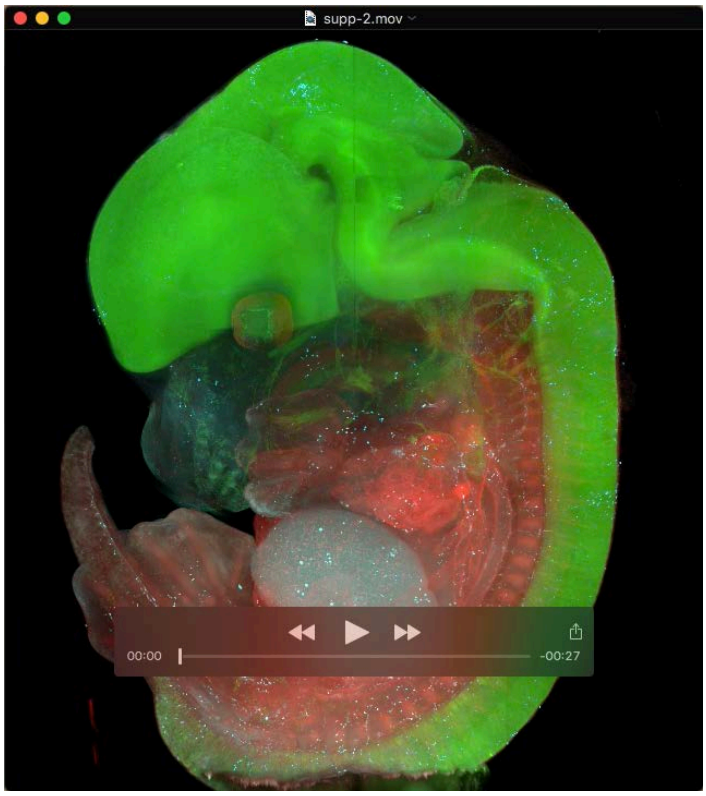

Movie 1. Whole embryo imaging of E13.5 *TRiCK* embryo.

Three-dimensional reconstruction of E13.5 *TRiCK* embryo cleared by IMES.

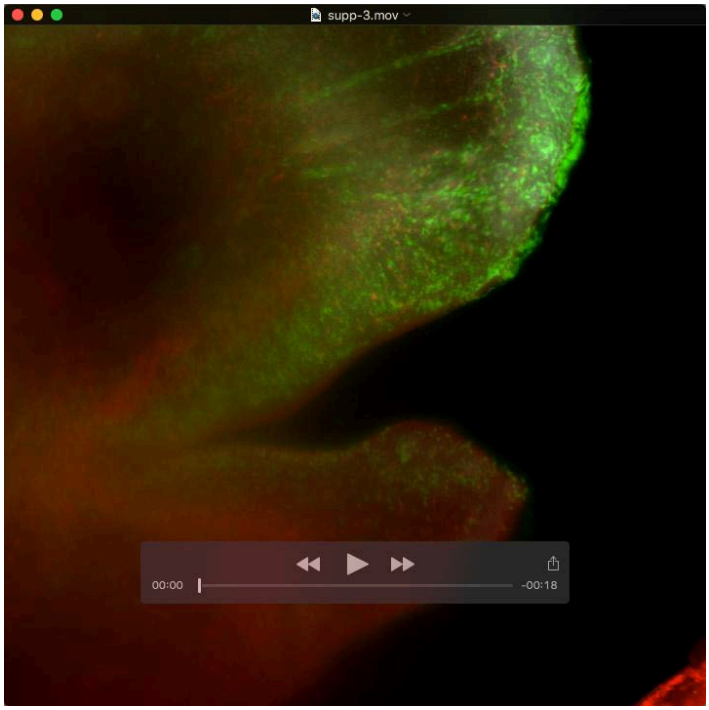

Movie 2. Sagittal view of the tongue and circumoral tissues of E14.5 *TRiCK* embryo.
The cleared E14.5 *TRiCK* embryo was virtually sectioned on lightsheet microscope.